non-quasi-static channel. In fact, the proposed linear decoder also has complexity of the order $O(QK)$ and reduces to the latter in the presence of block-fading channels.

Since orthogonal estimates of transmit symbols are obtained with the proposed combiner even in the presence of channel variations within encoding blocks, symbol-by-symbol maximum likelihood is achievable with significantly lower complexity compared to a strict maximum likelihood decoder. Given its low complexity and good performance, the proposed linear maximum likelihood decoder is suitable for implementation in lowcost, small, portable terminals, enabling OFDM systems to employ space–time transmit diversity on the downlink to mobile units, which is known to be a bottleneck of high-data-rate mobile wireless systems. Moreover, since the method presented reduces to the optimal linear technique known for the block-fading case, the proposed decoder can be used to support seamless indoor-to-outdoor transition in high-data rate wireless network services ('hot-spots').

Simulation results were presented which demonstrate the performance improvement offered by the proposed decoder, compared to other known linear decoders with similar complexity. It was also shown that in typical fading scenarios, the performance achieved with the proposed linear decoder is close to that of a strict maximum likelihood decoder. Therefore, the proposed decoder offers a low-cost alternative to nonlinear maximum likelihood decoding which might be impractical especially if QAM constellations (common in OFDM systems) and codes with higher diversity orders are employed.

We hope this work will inspire the pursuit of similar solutions for other STBCs already proposed [21–24], as well as others still to be discovered.

Although actual performance is dependent on the accuracy of channel estimation, as is the case of all coherent decoding schemes (including strict maximum likelihood), the correlation between time- and frequency-domain fading processes observed in OFDM channels can be exploited to yield low-complexity, accurate channel estimation for OFDM systems [14, 15]. Indeed, the work presented here can be combined with these low-complexity channel estimation techniques for OFDM systems, so as to yield iterative decoding/channel estimation algorithms which exploit the knowledge of channel states not only at pilot symbols, but at decoded symbols. Further investigations on this matter are currently being carried out by the authors.

7 Acknowledgment

The authors would like to thank Mr. C.J. Mitchell for his assistance in proofreading this manuscript.

8 References

1 Alamouti, S. M.: 'A simple transmit diversity technique for wireless communications', *IEEE J. Sel. Areas Commun.*, 1998, **11**, (8), pp. 1451–1458
2 Tarokh, V., Jafarkhani, H., and Calderbank, A.R.: 'Space-time block codes from orthogonal designs', *IEEE Trans. Inf. Theory*, 1999, **45**, (5), pp. 1456–1467
3 Tarokh, V., Jafarkhani, H., and Calderbank, A.R.: 'Space-time block coding for wireless communications: Performance results', *IEEE J. Sel. Areas Commun.*, 1999, **17**, (2), pp. 451–460
4 Tarokh, V., Seshadri, N., and Calderbank, A.R.: 'Space-time codes for high data rate wireless communications: Performance criteria in the presence of channel estimation errors, mobility and multiple paths', *IEEE Trans. Commun.*, 1998, **47**, (2), pp. 199–207
5 Firmanto, W., Vucevic, B., Yuan, J., and Chen, Z.: 'Space-time turbo trellis coded modulation for wireless data communications', *EURASIP J. Appl. Signal Process.*, 2002, **2002**, pp. 459–470
6 Li, X., Luo, T., Yue, G., and Yin, C.: 'A squaring method to simplify the decoding of orthogonal space-time block codes', *IEEE Trans. Commun.*, 2001, **49**, (10), pp. 1700–1703
7 Cimini, L.J.: 'Analysis and simulation of a digital mobile channel using orthogonal frequency division multiplexing', *IEEE Trans. Commun.*, 1985, **33**, (7), pp. 665–675
8 Cheng, J., Wang, H., and Cheng, S.: 'Space-time block coded transmit diversity for OFDM systems in mobile channels'. Proc. IEEE Personal, Indoor and Mobile Radio Communications (PIMRC'02), Lisbon, Portugal, 15–18 Sept. 2002
9 Li, Y.G., Chuang, J.C., and Sollenberger, N.R.: 'Transmitter diversity for OFDM systems and its impact on high-rate data wireless networks', *IEEE J. Sel. Areas Commun.*, 1999, **17**, (7), pp. 1233–1243
10 Liu, Z., Giannakis, G.B., Barbarossa, S., and Scaglione, A.: 'Transmit antennae space-time block coding for generalized OFDM in the presence of unknown multipath', *IEEE J. Sel. Areas Commun.*, 2001, **19**, (7), pp. 1352–1364
11 Lee, K.F., and Williams, D.B.: 'A space-frequency transmitter diversity technique for OFDM systems'. Proc. IEEE Global Telecommunications Conf. (Globecom'03), San Francisco, USA, 27 Nov. –1 Dec. 2003, pp. 1473–1477
12 Liu, Z., Ma, X., and Giannakis, G.B.: 'Space-time coding and Kalman filtering for time-selective fading channels', *IEEE Trans. Commun.*, 2002, **50**, (2), pp. 183–186
13 Edfors, O., Sandell, M., van de Beek, J.J., Wilson, S.K., and Borjesson, P.O.: 'OFDM channel estimation by singular value decomposition', *IEEE Trans. Commun.*, 1998, **46**, (7), pp. 931–939
14 Chang, M.-X., and Su, Y.T.: 'Model-based channel estimation for OFDM signals in Rayleigh fading', *IEEE Trans. Commun.*, 2002, **50**, (4), pp. 540–544
15 Deneire, L., Vandenameele, P., van der Perre, L., Gyselinckx, B., and Engels, M.: 'Space-time diversity systems based on constellation precoding', *IEEE Trans. Commun.*, 2003, **51**, (2), pp. 135–140
16 Tarokh, V., and Jafarkhani, H.: 'A differential detection scheme for transmit diversity', *IEEE J. Sel. Areas Commun.*, 2000, **18**, (7), pp. 1169–1174
17 Jafarkhani, H., and Tarokh, V.: 'Multiple transmit antenna differential detection from generalized orthogonal designs', *IEEE Trans. Inf. Theory*, 2001, **47**, (6), pp. 2626–2631
18 Lee, J.S., and Miller, L.E.: 'CDMA Systems Engineering Handbook' (Artech House, Boston, London, 1998)
19 Jakes, W.C.: 'Microwave mobile communications' (Wiley, New York, NY, USA, 1974)
20 Proakis, J.G.: 'Digital communications' (Mc-Graw-Hill, New York, NY, USA, 2000, 4th edn.)
21 Jafarkhani, H.: 'A quasi-orthogonal space-time block code', *IEEE Trans. Commun.*, 2001, **49**, (1), pp. 1–4
22 Ming, C., Tao, W., and Kangsheng, C.: 'A simple design method of orthogonal/quasi-orthogonal space-time block codes'. Proc. IEEE 14th Int. Symp. on Personal, Indoor and Mobile Radio Communications (PIMRC'03), Beijing, China, 7–10 Sept. 2003
23 Tirkkonen, O., and Hottinen, A.: 'Square-matrix embeddable space-time block codes for complex signal constellations', *IEEE Trans. Inf. Theory*, 2002, **48**, (2), pp. 384–395
24 Hassanpour, N., and Jafarkhani, H.: 'A class of full diversity space-time codes'. Proc. IEEE Global Telecommunications Conf. (Globecom'03), San Francisco, CA, USA, Dec. 2003

PAPER Special Issue on Ultra Wideband Systems

Adaptive RAKE Receivers with Subspace-based Hadamard-Hermite Template Design for UWB Communications

Craig MITCHELL†, Giuseppe ABREU†*, *Nonmembers, and* Ryuji KOHNO†, *Fellow*

SUMMARY In this paper we present a novel method for improving RAKE receiver reception in UWB systems. Due to the fact that practical pulses that can be produced for UWB-IR (Ultra Wideband - Impulse Radio) may be longer in time than the typical multipath resolution of the UWB channel, multiple channel components may occur within the typical pulse width. Performance degradation may occur due to the resulting intrapulse (overlapping received pulses) interference. We here propose a pilot aided RAKE receiver for UWB communications in the multipath environment present. The proposed system estimates the actual received signal with intrapulse interference in each RAKE finger using projections onto a Hadamard-Hermite subspace. By exploiting the orthogonality of this subspace it is possible to decompose the received signal so as to improve the template waveform and reduce the intrapulse interference. Using the projections onto the subspace the dimension of the received signal is effectively increased allowing for adaptive correlator template outputs. RAKE receivers based on this proposal are designed which show significant performance improvement and require less fingers than the conventional system to achieve required performance levels.

key words: Ultra Wideband, RAKE receiver, multipath, Orthogonal Hermite pulses

1. Introduction

UWB systems have become a popular topic of research as they promise very high speed wireless communications with many advantages over conventional radio systems [1,2]. Such systems offer the possibility of very low cost, high speed links over a short range ($< 10m$). Such links are hoped to support transmissions such as digital video and do away with unsightly and inconvenient cables. Further possible applications include sensor networks and Personal Area Networks.

Typically such systems communicate using trains of very short (1ns or less) pulses with a very low duty cycle. The energy is thus spread over a wide range of frequencies or bandwidth, resulting in a low power density at any single frequency. The extremely wide bandwidth gives UWB systems their strength. One problem, however, is that the received signal suffers from a significant multipath environment with relative path delays that are shorter than the duration of a typical realistic pulse ([3–6]). This fact will lead to severe intrapulse interference, as received pulses will overlap due to the close arrival times of the multipath components, which in turn will adversely affect the performance of any correlation based receiver.

The high degree of path diversity that is present, on the other hand, can be utilized and exploited by a RAKE like structured receiver (eg: [7,8]). Due to the fact that the inter-arrival times of the multipath components are not integer multiples of the pulse width, only a highly complicated fractionally spaced (FS) receiver utilizing maximum likelihood (ML) detection can compensate for the intrapulse interference that will be observed [8]. The problem with such receivers is that they require sampling at least at the Nyquist rate (which is impractically high in UWB systems as it may be in the order of tens of Gigahertz). They also require perfect knowledge of the multipath components amplitudes and arrival times and will therefore require complex channel estimation algorithms for any realistic implementation within the near future.

One alternative option recently considered to improve this situation is to use the Transmitted Reference (TR) system ([9,10]), where pulses are transmitted in pairs, an unmodulated reference followed by the modulated data pulse. The resulting received reference waveform is stored and used as the correlation template for the following modulated data pulse. Such a system is seen to be quite energy inefficient as two pulses are needed per data symbol. In addition the reference received waveform needs to be stored in an analog manner for correlation with the modulated pulse. This may also be impractical and inefficient.

Simplified RAKE receivers are therefore still a definite candidate for UWB transmission, but will suffer not only from relatively high complexity (due to the number of fingers and correlators required) but also from inefficient energy capture due to intrapulse interference. In this paper we propose a fingerwise modification to the RAKE receiver which attempts to overcome this intrapulse interference.

Orthogonal pulse designs such as those based on Hermite functions have been proposed for use in UWB systems for implementing M-ary Pulse shape modulation (PSM) [11–13]. Use of such orthogonal pulse

†The authors are with the Graduate School of Engineering, Division of Physics, Electrical and Computer Engineering Yokohama National University

*Presently, the author is with the Center for Wireless Communications, University of Oulu, Finland

shapes are thought to be severely hampered by the multipath channel. Recently it is therefore thought that the use of these orthogonal pulses are impractical for PSM. We here propose an alternative application of such orthogonal functions for intrapulse interference compensation in a RAKE Receiver. A set of such orthogonal pulses form an orthonormal basis which can be exploited in many circumstances. Many signals can be approximately reconstructed by decomposition onto such an orthogonal basis. We therefore propose to decompose the received signal in a given multipath environment in each finger of the RAKE using a *Hadamard-Hermite subspace*. The decomposed signals therefore represent reconstructions of the actual received signal and in addition increase the dimension of the received signal (to the size of the subspace) and allow the receiver to adapt its correlator template to the actual received waveform. Instead of using the results of only one correlator for detection, use is made of a bank of correlators for each of the orthogonal functions. This can therefore be used to reduce the effect intrapulse (intra-symbol) interference and increase the effective energy captured by the system.

The remainder of the paper is organized as follows. In Section 2 we introduce a brief background to the problem and discuss some relevant issues. In Section 3 we present our proposed system, in section 4 we evaluate the performance of the system and present some simulation results and finally we conclude in section 5.

2. The Multipath Channel and RAKE Receivers

2.1 Channel Model

A major concern in the implementation of any UWB system is the effect the UWB multipath channel will have on the performance. Much work has been carried out on channel measurements and modeling (*e.g.* [4–6]). A model that appears to have been accepted at this stage has been proposed by the IEEE P802.15.3a working group [3]. This model is based on the Saleh-Valenzuela model [14] with a couple of alterations. The model demonstrates a clustering phenomena of the multipath components into a number of discrete clusters. Each cluster in turn consists of a number of rays arriving in a certain spread of time. In addition it has been observed that each cluster exhibits independent fading as well as each ray within the cluster. This fading has also been seen to follow a log-normal distribution. The phase is randomly distributed to ± 1 representing channel inversions that may occur due to reflections of the waves off any solid objects. The model is given by:

$$h(t) = X \sum_{l=0}^{L} \sum_{k=0}^{K} \alpha_{k,l} \delta(t - T_l - \tau_{k,l}), \qquad (1)$$

Channel	CM1	CM2	CM3	CM4
Distance (m)	0-4	0-4	4-10	
(Non) Line of sight	LOS	NLOS	NLOS	NLOS
τ_m (ns)	5.05	10.38	14.18	
τ_{rms} (ns)	5.28	8.03	14.28	25

Table 1 IEEE P802.15.3a working group channel model parameters, showing distance, Line of sight, Mean excess delay τ_m and RMS excess delay τ_{rms}

where $\alpha_{k,l}$ are the gain coefficients, T_l is the arrival time of the l^{th} cluster with $\tau_{k,l}$ being the relative arrival time of the k^{th} ray within that cluster (relative to the first arrival path within the cluster ($\tau_{0,1}$). Both the cluster arrival rate and ray arrival rate are exponentially distributed, and the multipath gain magnitudes X are log-normally distributed. 4 different models representing different distances of transmission with both LOS or NLOS ((Non)- Line of Site) have been proposed. Table 1 gives some of the most important channel parameters for these channel models labeled CM1-CM4.

In this work we will concentrate on channels CM1 and CM2, representing both LOS and NLOS channels with a typical transmission distance of 0-4 meters. These channels together with CM3 represent the most likely application scenarios considered here, while CM4 is a long range outdoor channel. CM2 and CM3 were found to have very similar performance, so only CM2 will be considered here. It is however noted that the same procedure can be applied to the other channel situations with similar improvements in performance. We consider a multipath channel produced from the above model. One interesting thing to note about the UWB channel is that the multipath is extremely dense, especially in the NLOS situation and may result in intrapulse interference. The pulse repetition time is considered to be much longer than the delay spread of the channel, thus avoiding intersymbol interference and giving a low probability of multiuser interference in the system.

2.2 RAKE Receivers

RAKE Receivers utilize the path diversity that is available from the multipath channel. This is achieved by splitting the received signal into a number of components (fingers). The conventional RAKE receiver consists of multiple correlators (termed fingers) which can extract the received signal at each correlation instant. Correlation is carried out using the expected received signal as the matched filter template. Conventionally each finger is matched to the time instant of one of the resolved multipath components of the channel obtained by accurate channel estimation. The outputs of the fingers are then given appropriate weights and combined, using appropriate combining methods, so as to obtain the advantages of multipath diversity [7, 8, 15–17].

Such a RAKE receiver can be implemented using a

matched filter followed by a tapped delay line combiner with j taps. The number of taps in such an implementation is equal to the number of fingers and determine the instant in time that the correlation result is measured [15]. The system can resolve multipath components whose delays differ by at least one chip duration T_c (the RAKE resolution), which is typically the width of the template function or pulse width. The output of the correlator is therefore sampled at the time positions of the RAKE fingers and combined appropriately.

The term all RAKE (ARake) refers to the a receiver with unlimited resources [16], i.e. limitless fingers and path resolution. It attempts to position a finger at each and every resolved arrival path at the receiver so as to capture all of the impinging energy. This type of receiver also requires instant reconfiguration of the fingers for whenever the channel changes. Such a system is extremely complex, utilizes a large amount of power and is rather impractical. In reality each finger is of the order of a pulse width which is typically much larger than the multipath resolution. The performance of the correlators would suffer due to the intrapulse interference that will result. One possible solution is to use many overlapping RAKE fingers, termed a Fractionally-Spaced RAKE (FSRake), and the transmission of multiple pilot symbols so as to estimate the relative delays and magnitudes of all the paths. This requires a large number of RAKE fingers and results in large complexity and energy issues in the combining procedure. Additionally overlapping fingers, as well as intrapulse interference will be limiting factors in such a receiver as the chip duration is equal to the correlator template pulse duration ($T_c = T_p$). A typical RAKE combiner is limited by power consumption, energy of the signals, design complexity and the channel estimation available.

Many reduced complexity RAKE designs exist, and in this paper we consider 2 broad types of reduced complexity RAKE receivers, namely the partial RAKE (PRake) and selective RAKE (SRake) [15]. The PRake assumes that the arrival time of the first path is known, the first finger is positioned at this instant and the rest of the fingers are then positioned at multiples of the finger resolution. The SRake first scans the multipath delay spread signal and selects the highest energy paths to position its fingers thereby capturing maximum energy for a given number of fingers.

In this paper we attempt to find an alternative solution to the typical RAKE receiver. We consider a system where perfect channel estimation is not available at the receiver. In addition we assume full independence between RAKE fingers, therefore no two fingers can overlap, implying a RAKE resolution that is equal to the pulse width. Effectively this is a situation when the RAKE resolution is lower than the multipath resolution. We also assume that the system uses maximum-ratio combining [18].

3. Proposed System

As mentioned before orthogonal pulse shapes and PSM have been proposed for use in UWB systems. Use of such orthogonal pulse shapes may be hampered by the multipath channel. The overlap of pulses due to the intrapulse interference will lead to severe loss of orthogonality and thereby, it is thought, render any PSM system useless. The feasibility of PSM seems to only be realizable when extremely short duration pulses (shorter than the multipath resolution - possibly some 10's of picoseconds) can be produced, thereby avoiding intrapulse interference and maintaining orthogonality. In this paper we will however show that such pulse shaping may still prove useful in detection for UWB systems.

3.1 RAKE Fingers

We propose a finger-wise modification of the RAKE receiver based on the decomposition of received signals using a Hadamard-Hermite orthonormal basis.

We assume that the transmitted pulse ω_{TR} is the traditional 1-st order Hermite pulse. Antenna effects are ignored or assumed to be compensated for (e.g. differentiating effects are compensated by the inclusion of integrators), so the received waveform $\omega_{RC} = \omega_{TR}$. It is noted that the transmit and receive antennas are known to differentiate the signal [12] (implying a second derivative received waveform), while the channel is believed to have an integration effect [19]. This means that we cannot produce any pulse lower than 0-th order and therefore cannot receive one lower than 1-st order. This motivates the use of the 1-st order pulse here.

Using the 1-st order waveform means that the conventional RAKE receiver matched filter template function

$$T(t) = \omega_{RC}(t). \tag{2}$$

The proposal here is for a finger-wise improvement for the RAKE structure to the system. Each finger in the RAKE receiver will follow the modifications that are described for a single major RAKE finger. This major finger is defined as one that is centered on the maximum magnitude received path for any given instance of the IEEE channel model.

The received signal in the absence of noise $p(t)$, for a finger of pulse length T centered at time t_0 is defined as

$$p(t) = \sum_{k=1}^{v} \alpha_k \omega_{RC}(t - t_m - \tau_k) \quad \tau \in \left[\frac{T_p}{2}; \frac{T_p}{2}\right], \tag{3}$$

where v is the number of multipath components arriving in the duration of the finger (T_p) and α_k and τ_k represent the weights and relative delay of the k-th arrival path. t_m represents the mismatch between transmitter

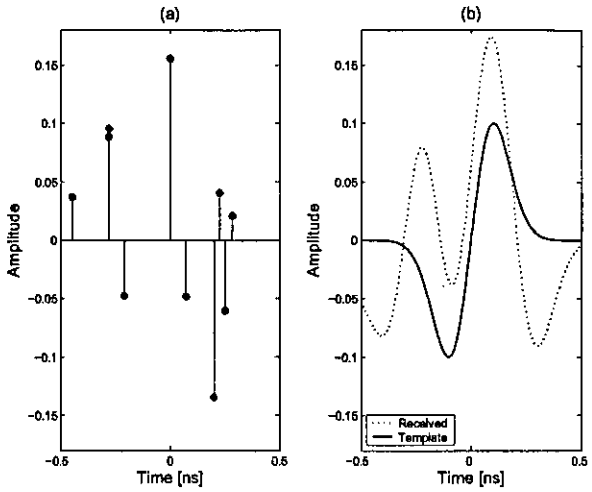

Fig. 1 (a) Example of major RAKE finger showing amplitudes and relative delays of the multipath components, (b) resulting noiseless received waveform ($p(t)$) and correlator template $T(t)$ in the major RAKE finger for channel shown in (a)

and receiver clocks. We assume perfect synchronization, so $t_m = 0$.

Figure 1 (a) shows an example of the multipath channel components contained in the major RAKE finger centered on the strongest multipath component and (b) shows the resulting received signal ($p(t)$) (composed of the weighted sum of shifted ω_{RC}) in the absence of noise for this finger. Also shown is the conventional RAKE finger template function $T(t)$ for comparison. As is seen multiple components may arrive within the pulse width of such a system (here assumed to be $T_p \approx 1ns$).

The RAKE finger performs detection by correlating the received waveform with the expected template ($T(t)$).

$$\gamma(t) = \int_{-\frac{T}{2}}^{\frac{T}{2}} p(t)T(t-\tau)d\tau. \tag{4}$$

If we consider Antipodal Binary Pulse Amplitude Modulation (BPAM) (i.e. a "1" is represented by $\omega_{TR}(t)$ and a "0" by $-\omega_{TR}(t)$. Detection can then be carried out as follows:

$$n_i = \begin{cases} 1 & \text{if} \quad \gamma(t) \geqslant 0 \\ 0 & \text{if} \quad \gamma(t) < 0 \end{cases} \tag{5}$$

The intrapulse interference can clearly be seen to have an effect on the performance of such a correlation procedure as the template $T(t)$ is not matched to $p(t)$, especially in the presence of noise. The closer the template $T(t)$ represents the actual noiseless received signal $p(t)$ the better the performance would be, as optimal performance is achieved when the signals match exactly.

3.2 Hadamard-Hermite Decomposition

The proposal in this paper is to use a Hadamard-Hermite subspace to decompose the received signal and more closely match the template to it.

Let the n-th order Hermite polynomial be defined in the interval $-\infty < t < \infty$ of a normalized time scale by the Rodrigues formula as follows [21]

$$P_n(t) \equiv (-1)^n e^{t^2} \frac{d^n}{dt^n} e^{-t^2} \quad n \in \mathrm{N}. \tag{6}$$

The normalized orthogonal Hermite pulses ψ_n are then defined by [12]:

$$\psi_n(t) = \frac{e^{\frac{-t^2}{2}} P_n(t)}{\sqrt{2^n n! \sqrt{\pi}}}. \tag{7}$$

where n is the order of the polynomial, and $n = 0, 1, \ldots, -\infty < t < \infty$. These are orthogonal in time and have a number of attractive attributes. They are based on smooth functions which implies they can be feasibly produced, they are also well contained in both frequency and time. In addition closed form expressions for the cross correlation function for any pair (n, m) of such functions has also been found [12]:

$$\begin{aligned} & R_{n,m}(\tau) \\ & = \int_{-\infty}^{\infty} \psi_n(t)\psi_m(t-\tau)d\tau \qquad (8) \\ & = \frac{(-1)^{2m+n}\tau^{m+n}\sqrt{n!m!}}{\sqrt{2^{m+n}}} e^{\frac{-\tau^2}{4}} \sum_{k=0}^{\lfloor (m,n) \rfloor} \frac{(-1)^k \tau^{-2k}\sqrt{4^k}}{(n-k)!(m-k)!k!} \end{aligned}$$

where $\lfloor (m,n) \rfloor$ denotes the minimum between n and m.

We further define the basis of Hadamard-Hermite pulses as follows. Consider an $n \times n$ Hadamard matrix $H = h_{i,j}$ where the entries $h_{i,j}$ are either $+1$ or -1 such that $HH^T = I^n$ where H^T is the transpose of H and I^n is the nth order identity matrix. Such a matrix H is defined as the nth order Hadamard matrix. The order of such a matrix is limited to 1, 2 or $4n$ where n is an integer. Given a Hadamard matrix H of order N, the normalized Hadamard-Hermite pulse is therefore defined as:

$$\varphi_n(t) = \frac{1}{\sqrt{N}} \sum_{k=0}^{N-1} h_{n,k}\psi_k(t), \tag{9}$$

Given the orthogonality of both H and $\psi_n(t)$ it follows that

$$\int_{-\infty}^{\infty} \varphi_m(t)\varphi_n(t)dt = \begin{cases} 0 & \text{if} \quad n \neq m \\ 1 & \text{if} \quad n = m \end{cases} \tag{10}$$

These Hadamard-Hermite pulses therefore form an orthonormal basis which we will refer to as the *Hadamard-Hermite space*. The reason for using Hadamard-Hermites, as apposed to plain Hermites is to do with the effective utilization of energy and will become evident when the signal detection is considered in the next subsection. An improved template function ($T^*(t)$) which more closely approximates $p(t)$ can now be found if the projections of the received signal onto this Hadamard-Hermite space are used. Mathematically

$$p(t) \approx T^*(t) = \sum_{k=0}^{N-1} c_k \varphi_k(t). \tag{11}$$

The coefficients c_k are seen to be the cross correlation between the received signal $p(t)$ and the k-th order Hadamard-Hermite pulse $\varphi_k(t)$, i.e.

$$c_k = \int_{-\infty}^{\infty} \varphi_k(t) p(t) dt. \tag{12}$$

Solving this equation using equation (8) we find that the decomposed pulse more closely represents the received signal than the conventional $T(t)$. Figure 2 (a) illustrates the reconstruction $T^*(t)$ of the received waveform $p(t)$, which was used in figure 1, using different dimensions of Hadamard-Hermite space. As can be seen the waveforms obtained far closer resemble the actual $p(t)$ when compared to the conventional Template. For correlation purposes it can be seen that these waveforms are far more useful and would lead to improved performance when compared to the conventional template. Figure 2 (b) shows a plot of the average relative square error in the reconstructed wave obtained from the major RAKE finger using 100 realizations of the IEEE channel model with CM1. Relative square error RSE, is calculated for sampled versions of p and T^* (with k samples) using,

$$RSE(T) = \frac{|p - T^*|}{|r|} = \sqrt{\frac{\sum_{j=0}^{k-1} (p(j) - T^*(j))^2}{\sum_{j=0}^{k-1} p(j)^2}}. \tag{13}$$

It is seen that the larger the dimension of the Hadamard-Hermite space the closer the reconstructed wave $T^*(t)$ resembles $p(t)$ and the lower the relative error is.

3.3 Signal Detection

The single matched filter of the RAKE Receiver is replaced with a bank of M correlators (each one consisting of a Hadamard-Hermite pulse from a dimension M Hadamard-Hermite space). We once again assume that

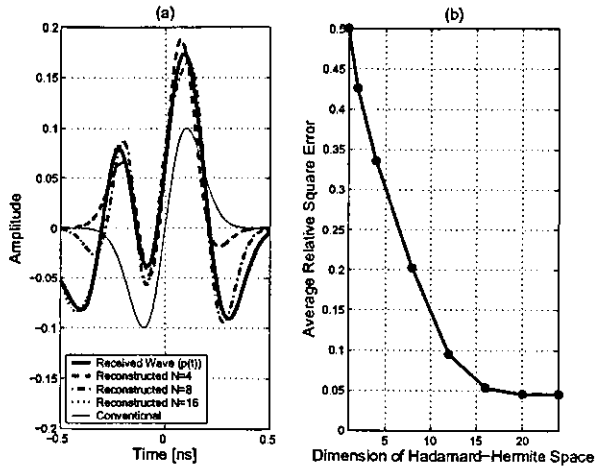

Fig. 2 (a) Reconstruction of $p(t)$ using Hadamard-Hermite space and (b) The average relative error in the reconstructed waveform in the major RAKE finger for different dimensions of Hadamard-Hermite space

BPAM modulation is being used. In the ideal noiseless case we see from equation (12) that the outputs of these correlators to an input $\omega_{RC}(t)$ would be,

$$\mathbf{c} = \{c_0, c_1, \ldots, c_{M-1}\}, \tag{14}$$

and if the input was $-\omega_{RC}(t)$ we would get $-\mathbf{c}$. In reality of course the system experiences noise and other distortions in the channel and receiver hardware resulting in an actual received signal:

$$r(t) = p(t) + w(t) \tag{15}$$

where $w(t)$ is the additive noise and other interference. The outputs of the correlators would now be:

$$\mathbf{d} = \{d_0, d_1, \ldots, d_{M-1}\}, \tag{16}$$

where

$$d_k = \int_{-\infty}^{\infty} \varphi_k(t) r(t) dt. \tag{17}$$

The proposed system uses the data-aided (DA) approach, where a number of known pilot symbols are transmitted at the beginning of the packet to estimate $\mathbf{c}$. The rest of the packet is decoded based on this estimated information. This is in accordance with the IEEE P802.15.3 UWB channel model which states that the channel is assumed to be time-invariant during the transmission of one packet if it is shorter that 200μs. Channel realizations are also assumed to be independent between packets. Using $\mathbf{c}$ as the reference detection can now be carried out as follows:

$$n_i = \begin{cases} 1 & \text{if } \mathbf{c} \cdot \mathbf{d}^T \geqslant 0 \\ 0 & \text{if } \mathbf{c} \cdot \mathbf{d}^T < 0 \end{cases} \tag{18}$$

The dimension of the detection is effectively increased,

as the outputs of all the M correlators are used in detection. This is advantageous to the performance of the system as was shown in [12].

3.4 Energy and Hadamard-Hermites

At this stage comment should be made about the use of a bank of Hadamard-Hermite as apposed to plain Hermite correlators. One undesirable consequence of using plain Hermite functions would be the sub utilization of the available energy. If we consider the "ideal" case where we have only one arriving pulse centered in the finger. If ω_{RC} is the 1-st order Hermite pulse, then only one of the correlators in the bank of Hermites would output a value (i.e. c_1). All others would have zero outputs, which is sub-optimal, even though a single pulse centered within a finger should intuitively be the best situation. Under the same conditions, the Hadamard-Hermite bank would have non-zero output values on all its correlators.

An alternative explanation can be seen by looking at the decision process. Errors are effectively determined by the distance between the detection vector $\mathbf{c}$ and the vector of noise processes ω_n at each correlator output, i.e. the metric:

$$\Delta(\mathbf{c}, \sigma_\omega) = E\left[\left|\left|\sum_{n=0}^{M-1} c_n\right| - \left|\sum_{n=0}^{M-1} \omega_n\right|\right|\right], \qquad (19)$$

where $E[\cdot]$ denotes expectation and it is assumed that all ω_n are independent zero mean Gaussian processes with variance σ_ω. Figure 3 gives a plot of these metric distances comparing Hermites and Hadamard-Hermites at different SNR values obtained by measuring the average distance in the major RAKE finger considering 100 channel instances of CM1. It is clearly seen that the plain Hermites suffer from suboptimal utilization of the energy. The Hadamard-Hermite solution maintains the mean distance regardless of the number of elementary shapes used. The advantages of the Hadamard-Hermite are therefore clear.

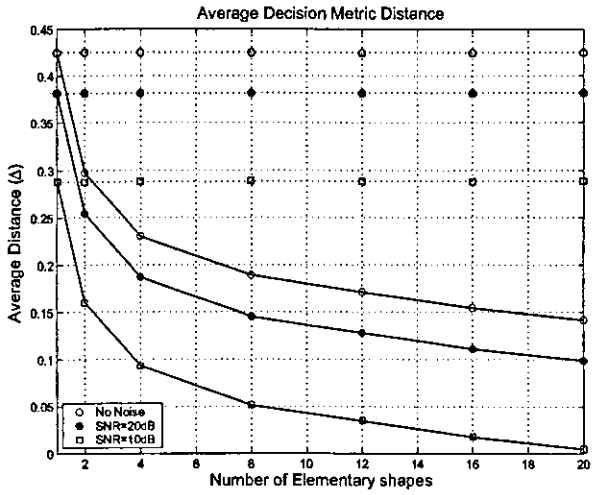

Fig. 3 Mean Decision Metric Distance for plain Hermite (solid lines) and Hadamard-Hermites (dashed lines) with differing SNR values

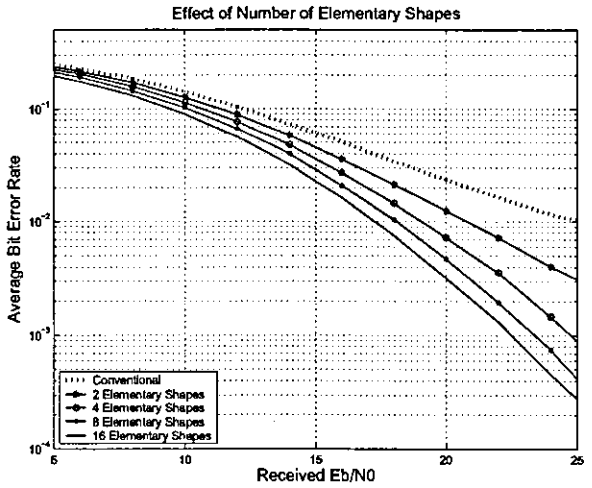

Fig. 4 Average Bit Error rate for major RAKE finger with increasing Hadamard-Hermite Dimension

3.5 Subspace Size

We assume initially that perfect knowledge of the reference vector $\mathbf{c}$ is available. This can be obtained by transmitting suitable pilot symbols as will be seen in the next subsection. The payload length of each data packet is assumed to be 1024 bits.

One problem of course is the larger the size of the Hadamard-Hermite subspace, the more complex the resulting pulse shapes become (more zero crossings in a short space of time), which may prove difficult and impractical to accurately produce in reality. Using a very large subspace size may unnecessarily increase the complexity of the system implementation. The effect of subspace size on the performance of the system needs to be investigated. To this end a system with a single major RAKE finger as described before is considered.

Figure 4 shows the Bit Error Rate performance of such a system with different sizes of Hadamard-Hermite space. The Received E_b/N_0 against which error rates are plotted is defined as the ratio between impinging energy (*per bit*) onto the receive antenna and the total noise at the output of the correlators. It can be seen that using a larger number of Hadamard-Hermite pulses improves the performance. One thing to note though is that the improvement in performance between 8 elementary shapes and 16 elementary shapes is relatively small. The increased complexity in using 16 as apposed to 8 shapes may make this impractical in a real system. The use of 8 shapes is therefore seen

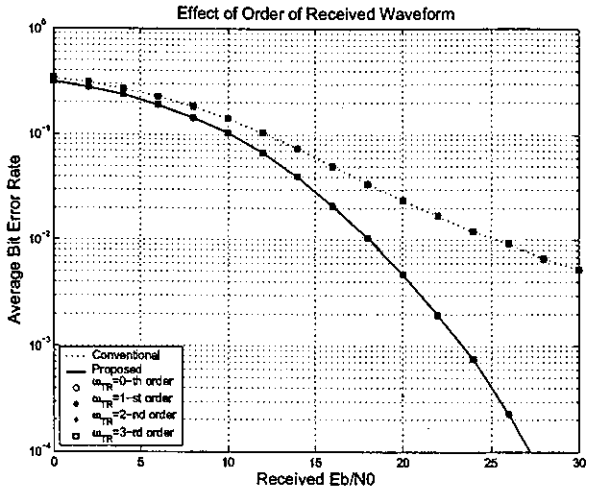

Fig. 5 Average Bit Error rate for major RAKE finger with increasing order of received waveform $\omega_{TR}(t)$ showing Conventional (dashed line) and Proposed system (solid line) using 8 elementary shapes

as a good compromise.

As mentioned we are considering a received waveform $\omega_{RC}(t)$ that is the standard 1-st order Hermite pulse. It is noted that this can be substituted for any other order Hermite pulse. Figure 5 shows the effect in BER in the major RAKE finger using increasing orders of received waveform $\omega_{TR}(t)$. As can be seen all the waveforms give virtually identical BER performance (They cannot be distinguished). The system here presented is largely independent of transmit pulse shape used (especially the Hermite pulses), and similar results are obtained when considering different shapes. Note these shapes may further be modulated so as to meet spectral requirements of local authorities.

3.6 RAKE Receivers

As mentioned before we concentrate on the reduced complexity RAKE receivers, namely PRake and SRake. The PRake is simply implemented assuming that the arrival time of the first multipath component is known (although this is not critical). The subsequent fingers are then just positioned at multiples of the finger width (in this case the pulse width, assumed to be 1ns).

The SRake proposed here requires some additional complexity in implementation. Firstly the energy output by the correlators in response to a pilot symbol are sampled at the resolution of the RAKE. Fingers are then positioned at maximum energy positions in descending order. When a limited number of fingers are available, the SRake may be advantageous as it would capture more of the available energy.

In contrast, the conventional SRake requires knowledge of the channel (or high accuracy channel estimation). After this such a system would position its fingers at the positions of the largest arrival paths, again in descending order. The requirement for perfect channel estimation may make such a system impractical in implementation.

3.7 RAKE Combining

If we consider a RAKE receiver with J fingers, we can obtain the well known expression for instantaneous signal to noise ratio (i-SNR) [17]:

$$\gamma_s = \rho \frac{E_s}{\sigma_s^2} \frac{(\sum_{j=1}^{J} a_j g_j)^2}{\sum_{j=1}^{J} g_j^2}, \tag{20}$$

where g_j represent the RAKE weights and depend on the combining techniques used. ρ is the normalized correlation of a single pulse. E_s is the symbol energy of the transmitted signal and E_s/σ_s^2 is therefore regarded as the SNR of the transmitted signal. a represents the magnitudes of the arrival paths. For a given finger which had v arrival paths of magnitude α within its duration (see equation 3), $a_j^2 = \sum_{i=1}^{v} \alpha_i^2$. The well known maximum ratio combining method (MRC) [17] can be obtained through applying the Cauchy inequality:

$$\gamma_s = \left(\sum_{j=1}^{J} a_j g_j \right)^2 \leqslant \sum_{j=1}^{J} a_j^2 \sum_{j=1}^{J} g_j^2, \tag{21}$$

which is equal only when $g_j = a_j$. The i-SNR for MRC is therefore:

$$\gamma_{s,MRC} = \rho \frac{E_s}{\sigma_s^2} \sum_{j=1}^{J} a_j^2, \tag{22}$$

3.8 Pilot Symbols

3.8.1 Correlator Estimation

For detection in the system (equation (18)) the receiver requires knowledge of the noiseless outputs of the correlators (vector $\mathbf{c}$) given by (14). This can be achieved by the transmission of suitable pilot symbols at the beginning of the packet. Naturally these symbols are transmitted in a noisy environment therefore only an estimate $\hat{\mathbf{c}}$ can be obtained.

One of the best methods for estimating values, vectors and/or functions in a noisy environment is the Kalman filter [20]. In this case it involves the simple case of measuring a fixed vector in noisy measurements using a Kalman filter. We use the following filter equations for k-th measurement from k pilot symbols:

$$K_k = \frac{P_{k-1}}{P_{k-1} + R} \tag{23a}$$

$$\hat{\mathbf{c}}_\mathbf{k} = \hat{\mathbf{c}}_{\mathbf{k-1}} + K_k(\hat{\mathbf{c}}_\mathbf{k}^* - \hat{\mathbf{c}}_{\mathbf{k-1}}) \tag{23b}$$

$$P_k = (1 - K_k)P_{k-1} \tag{23c}$$

where K is the filter gain, P is the error covariance

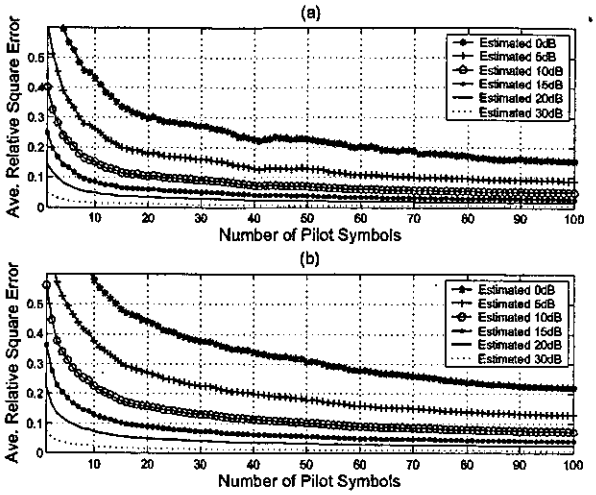

Fig. 6 Average Relative Square error versus number of pilot symbols k for RAKE fingers showing (a)4 Elementary Hadamard-Hermites and (b)8 Elementary Hadamard-Hermites

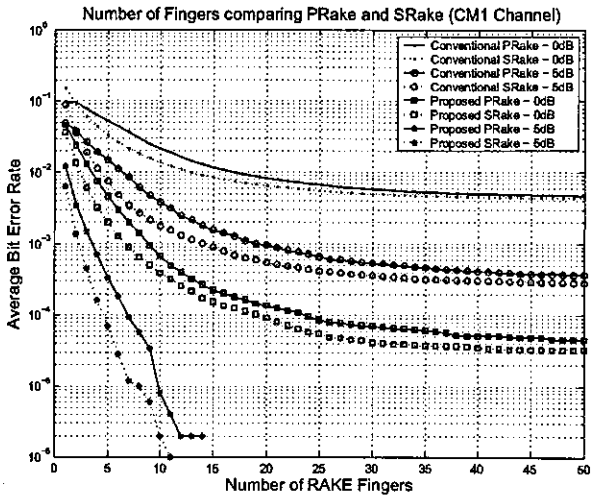

Fig. 7 Average Bit Error Rate performance comparing PRake (solid lines) and SRake (dotted lines) receivers on CM1 with increasing numbers of RAKE fingers at different i-SNR levels. Comparisons are also made of the conventional system with the proposed system using 8 elementary Hadamard-Hermite templates.

in the estimate (we assume an initial value of 1), R is the measurement variance (related to the noise variance and given an initial value of 0.5 so as to cover a wide range of SNR values). $\hat{\mathbf{c}}_\mathbf{k}^*$ represents the measurement (or output of the correlators) and $\hat{\mathbf{c}}_\mathbf{k}$ is the estimate in response to the k-th pilot symbol.

To find the optimum number of pilot symbols required we analyze the average relative square error:

$$RSE(\hat{\mathbf{c}}) = \frac{|\mathbf{c} - \hat{\mathbf{c}}|}{|\mathbf{c}|}. \tag{24}$$

Figure 6 shows the average relative square error for the estimated $\hat{\mathbf{c}}$ in the major RAKE finger at different values of i-SNR from equation 22. As can be seen the greater the number of pilot symbols the better the estimate of $\mathbf{c}$ becomes as the RSE reduces. By selecting a required RSE at a certain noise level we can find the optimum number of pilot symbols for the system. for example at 5dB noise and an RSE of 0.2 it can be see that 20 pilots are needed when 4 elementary Hadamard-Hermites, and 50 pilots when 8 elementary Hadamard-Hermites are used.

3.8.2 Energy Scanning

Pilot symbols are also required for finding the position of fingers in the SRake structure that is considered. The energy output by the correlators is measured and sampled at RAKE resolution to determine the best positions for the fingers of the SRake. Once again such pilots symbols are transmitted in a noisy environment. A small number of pilot symbols are required so as to satisfactorily position the SRake fingers. When multiple Pilot symbols are used, the energy measured at each sample time is simply averaged over the number of pilots used, and the positions of the RAKE fingers are determined.

4. Simulation Results

This section presents simulation results for a single user system on both CM1 and CM2. The pulse width is considered to be 1ns. The RAKE systems considered can only position the fingers at integer multiples of the pulse duration T (assumed to be 1ns). A PRake system with j fingers therefore assumes that the arrival time of the first multipath component is known as the position of the first finger, and the subsequent fingers are then positioned at integer multiples of T thereafter. For the SRake system the best j positions in terms of maximum energy capture by the given set of correlators are used. The packet size is set to 1024 bits.

4.1 Perfect Knowledge

At first we assume that the system has perfect knowledge of the vector $\mathbf{c}$, and is also able to position the fingers of an SRake receiver ideally.

Figure 7 shows the comparison in bit error rate (BER) performance of the conventional single template system and the proposed system considering both PRake and SRake structures. The channel considered is the LOS CM1 channel. The plot shows the effect of increasing the number of fingers has on the performance of the system at i-SNR (as defined by equation 22) values of 0 and 5dB's.

It can clearly be seen that an increase in the number of fingers has the effect of improving the perfor-

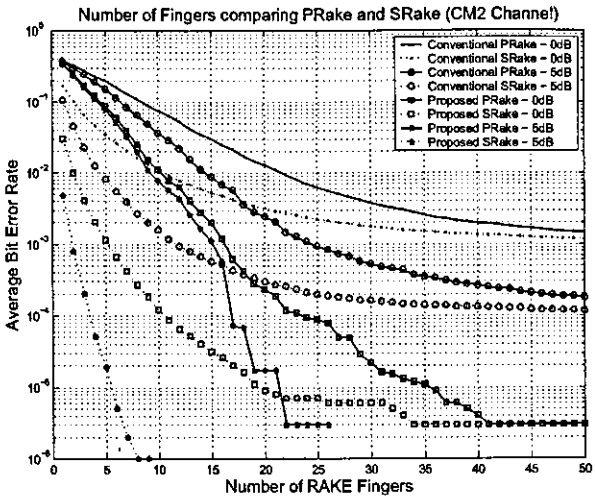

Fig. 8 Average BER comparing PRake (solid lines) and SRake (dotted lines) receivers on CM2 with increasing RAKE fingers at different i-SNR levels.

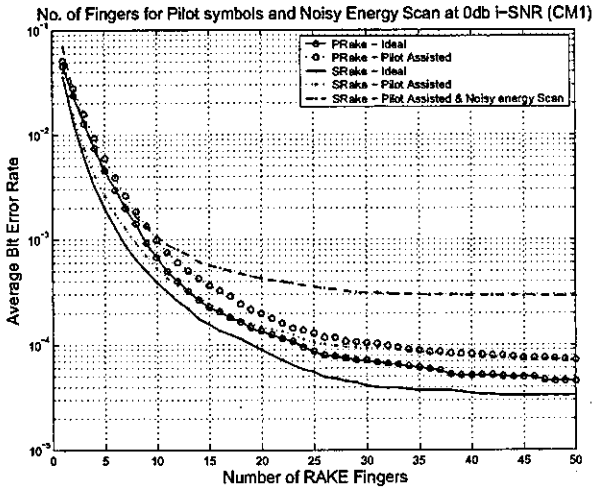

Fig. 9 Average BER showing the effect of using pilot symbols and energy scanning for the proposed PRake and SRake receivers on CM1 with increasing RAKE fingers at different 0dB i-SNR.

mance for all receivers considered. In addition to this it is also seen that the proposed RAKE finger structure outperforms the conventional system by a large margin. For example at an i-SNR of 0dB's, the proposed system has a BER that sits well below the conventional systems 5dB BER. Significant gains in performance are achieved when using the proposed Hadamard-Hermite space.

It is noted that there is an optimum number of fingers in the system. Increasing the number of fingers above about 25 shows no real significant improvement in the performance at any noise level. The reason here is that most of the significant multipath components that arrive at the receiver in the CM1 channel occur in the first 25ns. Thereafter the components which arrive are much weaker and have little effect on the performance (i.e. no significant improvements are evident).

Another important conclusion that can be drawn from this plot is that for a given number of RAKE fingers the SRake system will have a better performance than the PRake. Effectively, as can clearly be seen, the SRake requires less fingers to achieve a certain BER than the PRake does. In the LOS channel the major paths arrive very close to the beginning of the multipath spread so the gain achieved with a SRake receiver is not very significant.

Figure 8 now considers the same PRake and SRake structures on the NLOS channel CM2. Due to the absence of a direct LOS component and a denser multipath environment, it is seen that the PRake has a much more linear performance than observed in figure 7. Once again it is clear from the plot that the proposed system offers a significant improvement over the conventional RAKE receivers. In fact as observed the performance of the PRake in this CM2 channel is poor with a small number of fingers. This is due to the fact that the maximum arrival paths have less energy than those in CM1. It is however seen that with a larger number of fingers the performance improves considerably. This is due to there being more diversity in the fingers of the RAKE (higher density in multipath). Due to the fact that the finger resolution is 1ns in these simulations, the system is also capable of effectively utilizing more of the received energy when more paths are available in each finger.

It should also be noted that the arrival paths are not concentrated at the beginning of the multipath spread in this situation. A larger number of paths with an increased delay spread means that far more fingers are required in the PRake system to achieve a certain level of performance. In addition, the SRake is seen to have a large improvement in performance over the PRake in this channel situation. A significantly lower number of fingers is required to achieve the same performance. Once again this can be attributed to the increase in the path density and the fact that the most significant paths are not necessarily positioned near to the first arrival path. The added complexity of the SRake structure may well be considered acceptable due to the significant reduction in the number of fingers required.

4.2 Pilot Assisted

The more realistic situation needs to be considered where perfect knowledge of the correlator outputs or energy spread along the delay spread is not known. As has been mentioned pilot symbols are used at the beginning of each packet for this purpose. As stated 50 pilot symbols are used for estimating the vector **c**.

Figure 9 shows the effect of using Pilot symbols

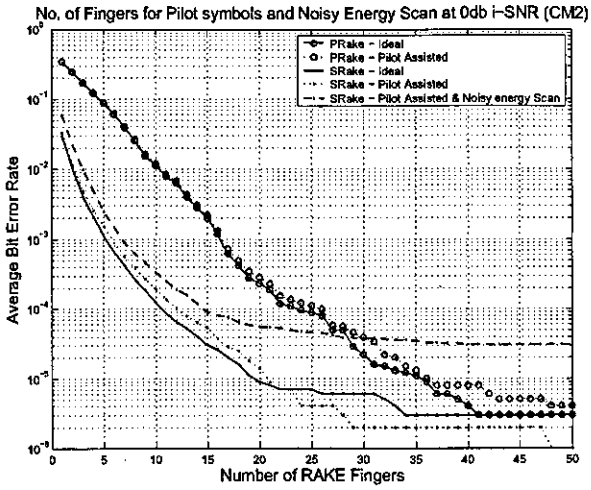

Fig. 10 Average BER showing the effect of using pilot symbols and energy scanning for the proposed PRake and SRake receivers on CM2 with increasing RAKE fingers at different 0dB i-SNR.

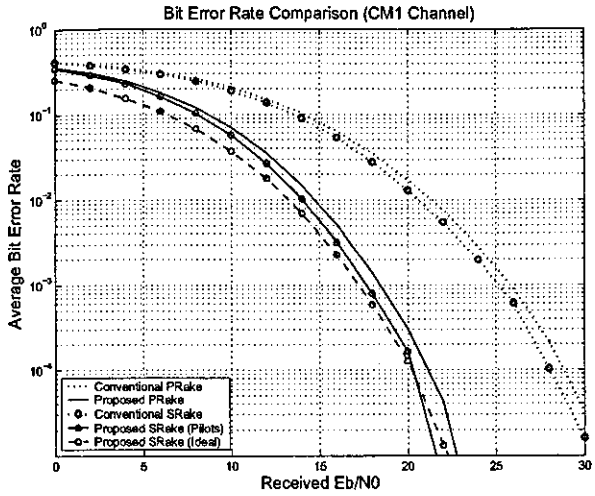

Fig. 11 Average BER PRake and SRake receivers on CM1 with 25 RAKE Fingers.

on both the proposed PRake and SRake structures on channel CM1. Results are shown at an i-SNR level of 0dB. As was seen in figure 7 the difference between PRake and SRake performance in CM1 is quite small. In fact, as can be seen, when the pilot symbols are included, the advantage of using the SRake is diminished even further. Figure 9 additionally shows the situation when a further 50 pilot symbols are used to find the positions of the SRake fingers (it has been found that using any more pilot symbols here makes very little difference). When this situation is considered, there is a significant reduction in performance, especially at these high noise levels. In fact it can be argued that the increased complexity of the SRake structure is not justified on CM1.

Figure 10 shows the same results obtained on CM2. Once again the slight loss in performance due to having to estimate $\mathbf{c}$ can be observed, as well as the loss in performance that one would observe when estimating the positions for the fingers in the SRake structure when using pilot symbols (once again 50 pilot symbols were used for this purpose). For CM2, as was seen previously, the use of the SRake structure is advantageous over the PRake.

The reduced performance that is observed when the energy scan is done in noise is due to the fact that the energy available in the fingers is small compared to the noise energy at this high noise level. When full Bite Error Rate simulations over a range of noise values are considered this problem is reduced as seen in the next subsection.

4.3 BER

We now consider the overall Bit Error Rate (BER) performance of the system. We consider the situation in terms of the received E_b/N_0. E_b is defined as the expected received energy per information bit that takes the IEEE channel model normalization into consideration as well as the loss due to using pilot symbols, i.e:

$$Loss = 10\log_{10}\frac{N_b}{N_b + N_{Pc} + N_{PE}}, \qquad (25)$$

where N_b is the number if information bits, N_{Pc} is the number of pilot symbols used to estimate $\mathbf{c}$ and N_{PE} is the number of pilot symbols used to position the fingers in the SRake structure.

Figure 11 shows a plot of the BER for PRake and SRake structures on CM1. As can be clearly seen the proposed RAKE finger structure shows vast performance improvements for both PRake and SRake receivers. In addition it is also evident that the difference in performance between the SRake and PRake receivers are relatively small. This is again due to the fact that most of the energy is contained within the first few tens of nanoseconds in the LOS CM1 channel. In addition plots for the proposed SRake structure showing the ideal situation, where perfect knowledge of $\mathbf{c}$ and perfect finger positioning is available, as well as the situation where pilot symbols are used to estimate $\mathbf{c}$ and finger positions. It is clear that a relatively small reduction in performance is caused.

The situation in the NLOS channel CM2 is different. The effect of increasing the number of fingers in the proposed system is illustrated in figure 12.It is again noted that the best performance is seen when 25 fingers are used. No significant improvement in performance is seen above this value. In fact slight reduction in performance is seen (this is due to the fact that finger positioning may not be perfect and the result is effected more by noise in fingers that are positioned incorrectly). It is also noted that as the number of fingers increases

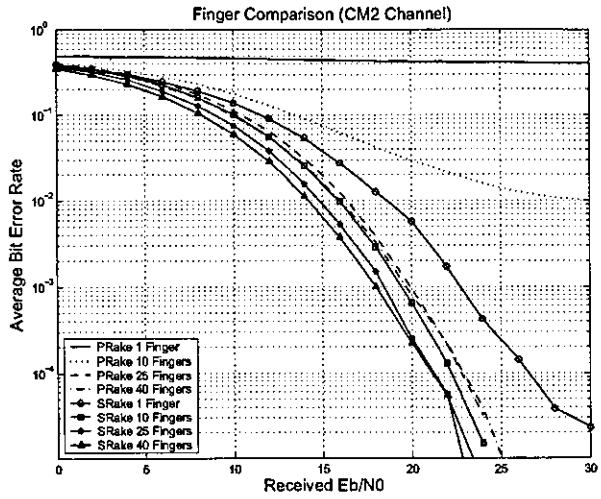

Fig. 12 Average BER for the Proposed PRake and SRake receivers on CM2 with increasing RAKE Fingers.

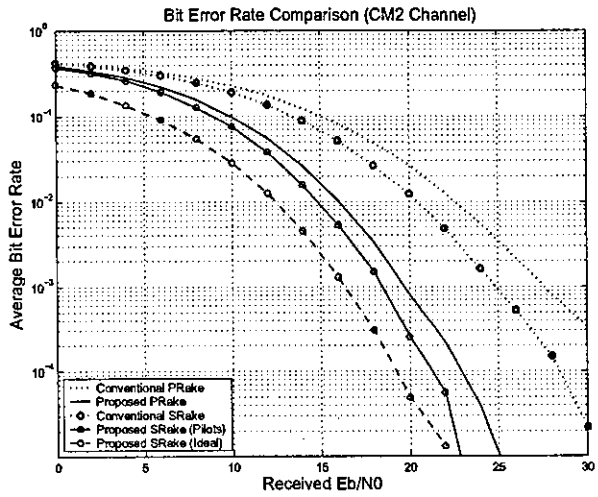

Fig. 13 Average BER PRake and SRake receivers on CM2 with 25 RAKE Fingers.

the performance of the SRake and PRake become a lot closer to each other. This is consistent with the results in the previous subsection. This does however emphasize the fact that when only a limited number of fingers are to be employed, the SRake outperforms the PRake, particularly with a low number of fingers.

Finally figure 13 compares the BER performance of the conventional and proposed receivers in the NLOS channel CM2. Once again the significant performance improvements with the proposed structure over the conventional structure can be seen. Improvement of more than 5dB is seen at many BER levels. With 25 fingers in CM2 it is seen that the SRake structure shows about a 2db performance advantage over the PRake structure. Once again the effect of the pilot symbols is also shown in the plot. The performance improvement obtained using the SRake structure is still seen as being advantageous in this situation. Further improvements can be obtained if coding and repetition were employed.

5. Conclusions

In conclusion this paper represented a novel finger-wise modification to the standard RAKE receiver. By using a Hadamard-Hermite base the proposed system showed significantly better performance than the conventional approach in simulation results. The effects of intrapulse interference due to the finger spacing being much larger than the typical multipath resolution can be reduced using this approach. Far fewer RAKE fingers would be required to obtain similar levels of performance to such a conventional system. Fewer RAKE fingers in the system may make it more practical to implement in reality.

It is also noted that the approach used here is largely independent of the shape of the transmitted waveform. This means that the same approach can be used for different transmit waveforms that are present. In addition it should also be noted that this approach may also be useful in combatting any other distortions that remain constant for the duration of the packet. This implies that any antenna distortion may also be compensated for in a similar fashion. The performance, under these circumstances needs to be investigated. In future we intend to analyze this as well as well as the possibilities of implementing different modulation schemes.

References

[1] M. Z. Win, and R. A. Scholtz, "Impulse Radio: How it works," *IEEE Communications Letters*, Vol. 2, pp. 36-38, Feb. 1998.

[2] M. Z. Win, and R. A. Scholtz, "Ultra-Wide Bandwidth Time-Hopping Spread-Spectrum Impulse Radio for Wireless Multiple-Access Communications," *IEEE Transactions on Communications*, Vol. 48, No. 4, pp. 679-691, April 2000.

[3] J.Forrester et al., "Channel modeling sub-comittee report final," *IEEE P802.15 Working Group for Wireless Personal Area Networks (WPANs)*, IEEE P802.15-02/490r1-SG3a, Feb. 2003.

[4] M. Z. Win and R. A. Scholtz, "Characterization of ultra-wide bandwidth wireless indoor channels: a communication-theoretic view," *IEEE J. Select. Areas Commun.*, vol. 20, no. 9, pp. 1613–1627, Dec. 2002.

[5] A. Álvarez, G. Valera, M. Lobeira, R. Torres, and J. L. García, "Ultrawideband channel characterization and modelling," in *Proc. IEEE 1st International Workshop of UWB Systems (IWUWBS'03)*, Oulu, Finland, June2-5 2003.

[6] J. Keignart and N. Daniele, "Channel sounding and modelling for indoor uwb communications," in *Proc. IEEE 1st International Workshop of UWB Systems (IWUWBS'03)*, Oulu, Finland, June2-5 2003.

[7] M. Win and G. Chriskos and N.R. Sollenberger, "Performance of Rake reception in dense multipath channels: implications of spreading bandwidth and selection diversity

order," in *IEEE JSAC*,Vol. 18, No. 2, August 2000, pp 1516-1525.

[8] B. Mielczarek and M. Wessman and A. Svensson, "Performance of coherent UWB rake receivers with channel estimators," *Vehicular Technology Conference 2003. VTC 2003-Fall*,Volume 3, 6-9 Oct. 2003 Pages:1880 - 1884

[9] S. Franz and U. Mitra, "Integration Interval Optimization and Performance Analysis for UWB Transmitted Reference Systems," in *Proc. IEEE Joint UWBST and IWUWBS04*, Kyoto, Japan, May 18-21, 2004.

[10] J. Romme and G. Durisi, "Transmit Reference Impulse Radio Systems Using Weighted Correlation," in *Proc. IEEE Joint UWBST and IWUWBS04*, Kyoto, Japan, May 18-21, 2004.

[11] C. J. Mitchell, G. Abreu and R. Kohno, "Combined Pulse Shape and Pulse Position Modulation for High Data Rate Transmissions in UWB Communications," *International Journal of Wireless Information Networks*, Number 10, Volume 4, page 167-178, October 2003.

[12] G. Abreu, C. J. Mitchell and R. Kohno,"On the Design of Orthogonal Pulse-Shape Modulation for UWB Systems Using Hermite Pulses", *JCN (Journal of Communications and Networks) Special Issue on Ultra-Wideband Communications*, vol. 5, no. 4, pp. 328-343, December 2003.

[13] M. Ghavami, L. B. Michael and R. Kohno, "Hermite Function Based Orthogonal Pulses for Ultra Wideband Communications," *Proceedings of the WPMC'01 - Aalborg, Denmark*, pp. 437-440, 2001.

[14] A. Saleh and R. Valenzuela, "A Statistical Model for Indoor Multipath Paropagation," in *IEEE JSAC*,Vol. SAC-5, No. 2, February 1987, pp 128-137.

[15] D. Cassioli and M. Win and F. Vatalaro and A.F Molisch, "Effects of Spreading Bandwidth on the Performance of UWB Rake Receivers," Mitsubishi Research Laboratory report, TR-3003065, August 2003.

[16] M. Win and Z.A. Kostic, "Virtual path Analysis of selective Rake receiver in dense multipath channels," in *IEEE Communications Letters*,Vol. 3, November 1999, pp 308-310.

[17] J. Zhang and R.A. Kennedy and T.D. Abhayapala, "Conditions and Performance of Ideal RAKE Reception for Ultra-Wideband Signals in Lognormal Fading Channels," *International Journal of Wireless Information Networks*, Number 10, Volume 4, page 193-200, October 2003.

[18] J. G. Proakis, *Digital Communications, Fourth Edition*. New York, NY: Mc-Graw-Hill, 2000.

[19] A. Armogida and B. Allen and M. Ghavami and M.Porretta and G. Manara and H. Aghvami, "Path Loss Modelling in Short Range UWB Transmissions," in *Proc. IEEE 1st International Workshop of UWB Systems (IWUWBS'03)*, Oulu, Finland, June2-5 2003.

[20] G. Welch and G. Bishop, "An Introduction to the Kalman Filter," *UNC-Chapel Hill*,TR 95-041, April 2004.

[21] A. D. Poularikas, *The Transforms and Applications Handbook, Second Edition*, 2nd ed. CRC Press, Feb.23 2000.

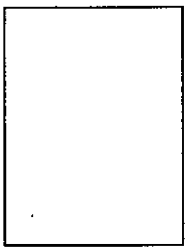

Craig John Mitchell was born in Johannesburg, South Africa in November 1975. He received both his B.Sc. (*summa cum laude*) and M.Sc. in electrical engineering from the University of the Witwatersrand - South Africa in 1997 and 2001, respectively. He is currently working towards his PhD at the Yokohama National University - Japan. His research interests lie in the areas of ultra-wideband systems, coding wireless communications. He was the recipient of the *Uenohara Foreign Student'S Award for Excellence in Research* in 2004.

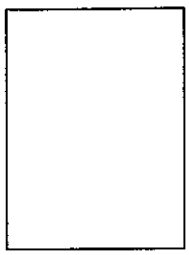

Giuseppe Abreu Giuseppe Abreu was born in Salvador-Bahia, Brazil in December 1972. He received his B.E. in electronics engineering from the Federal University of Bahia, Brazil, in 1996. From April, 1997 to March, 2004, he was a research with the Kohnolaboratory of the Yokohama National University, Japan, where he obtained his M.E. and Ph.D. degrees in electrical and computer engineering. He was also the recipient of the Uenohara Foreign Student's Award for Excellence in Research from the Tokyo University in 2000. He has authored and coauthored 2 internationally registered patents (for Sony Corporation, Japan), a few international journal papers and various conference papers. He is currently with the Center for Wireless Communications at the University of Oulu Finland. His current research interests include Smart Antennas, Beampattern Synthesis, Space-Time Signal Processing and Coding, MIMO Systems and Ultra Wideband Communications.

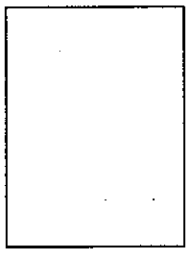

Ryuji Kohno was born in Kyoto, Japan in March 1956. He received his B.E. and M.E. degrees in computer engineering from Yokohama National University in 1979 and 1981, respectively, and Ph.D. degree in electrical engineering from the University of Tokyo in 1984. He joined the Department of Electrical Engineering, Tokyo University, in 1984 and was made an Associate Professor in 1986. From 1988-1997 he was an Associate Professor in the Division of Electrical and Computer Engineering, Yokohama National University, where he is now a Full Professor. He is the Chairman of the Societies of ITS and Software Radio of the IEICE, an Editor to the IEEE Transactions on Communications and on Information Theory, and of the IEICE Transactions on Fundamentals of Electronics, Communications, and Computer Sciences. His research interests lie in several areas of wireless, optical and cable communications, coding and information theory, spread spectrum and ultra-wideband systems, etc. He is a member of IEEE, EURASIP, IEICE, IEE and IPS of Japan and the author of several technical books and numerous papers.

On the Performance of Bit-Interleaved Coded DAPSK over Rayleigh Fading Channels

Koji Ishibashi, Hideki Ochiai, and Ryuji Kohno
Division of Physics, Electrical and Computer Engineering
Yokohama National University
79-5 Tokiwadai, Hodogaya-ku, Yokohama, 240-8501, Japan
email: koji@ieee.org

Abstract— **We analyze the achievable performance of the coded differential amplitude and phase shift keying (DAPSK) over a frequency non-selective Rayleigh fading channel with ideal bit interleaving. The bit metrics based on the exact probability density of detector output and the average mutual information of the system with conventional differential detection are derived and compared with that of multiple-symbol differential detection (MSDD). It is shown that by suitably incorporating the amplitude statistics of transmitted signals into bit metrics, the performance of conventional DAPSK can be significantly improved without increasing complexity. Theoretical framework developed above is also justified by the comparative simulation results using convolutional and turbo codes.**

I. Introduction

Due to its robustness against phase ambiguity induced by rapid fading with low complexity, the differential detection has been a preferable choice for mobile communication systems. The differential detection in its original form literally makes use of the difference, typically in the polar coordinates, between the two consecutive received symbols. Also, combined with the orthogonal frequency-division multiplexing (OFDM) signaling, the differential detection will enable one to cope with frequency-selective fading channels without accurate channel estimation, resulting in a very simple receiver structure [1].

While the differential detection scheme enjoys very low complexity and robustness against fading channels, its well-known drawback is the performance loss relative to coherent detection over static channels whenever an accurate reference symbol is available at the receiver. In contrast to the simple detection above, which will be referred to as *conventional differential detection* (CDD) in the following, more recent techniques such as *multiple symbol differential detection* (MSDD) [2] fully utilize all consecutive outputs of differentially encoded symbols based on a maximum-likelihood (ML) criterion. Therefore, MSDD significantly outperforms CDD over an AWGN and slow fading channels with an increase of receiver complexity.

In this paper, we focus on the bit-interleaved coded differential amplitude and phase shift keying (DAPSK) system, which is a differentially detectable modulation with potentially higher bandwidth efficiency than conventional DPSK. Although the performance of uncoded DAPSK has been studied well in the literature, the performance of coded DAPSK, especially in combination with CDD, has not been well addressed except for [3]. Thus, we first analyze the performance of bit-interleaved coded DAPSK based on CDD in terms of the average mutual information (AMI) over a frequency non-selective slow Rayleigh fading channel. The results are compared with that of MSDD [4], which will reveal that the performance loss of CDD with channel coding is in fact significant. Thus, we further develop a simple bit metric with CDD that can approach the performance of MSDD with lower complexity. The resultant metric also outperforms the suboptimal metric based on Gaussian approximation of noise terms proposed in [3] for a high signal-to-noise ratio (SNR) scenario.

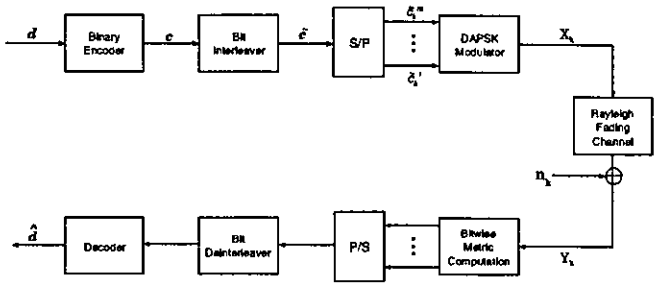

Fig. 1. System model of bit-interleaved coded DAPSK over block Rayleigh fading channels.

II. Bit-Interleaved Coded DAPSK

A. Transmitter Model

The overall system model is depicted in Fig. 1. At the transmitter, a binary information sequence $\boldsymbol{d}$ is encoded by the binary channel encoder. The resultant binary code word of length N, $\boldsymbol{c} = [c_1, c_2, \ldots, c_N] \in \{0,1\}^N$, is followed by the bit interleaver, which generates the bitwise interleaved sequence $\tilde{\boldsymbol{c}}$. Let $\mathcal{X}$ denote the set of constellation of complex signals with $|\mathcal{X}| = 2^m$. Each m-tuple of the bit interleaver outputs at time instant k, $\tilde{\boldsymbol{c}}_k = [\tilde{c}_k^1, \tilde{c}_k^2, \ldots, \tilde{c}_k^m]$, is then mapped to $X_k \in \mathcal{X}$. Since we apply differential encoding, the mapping should also depend on the previous symbol $\tilde{\boldsymbol{c}}_{k-1}$ or X_{k-1}.

The DAPSK constellation considered in this paper, also known as a star QAM, is a combination of 2^n-DASK and 2^{m-n}-DPSK constellations. The signal constellation set $\mathcal{X}$ of the DAPSK is composed of 2^n concentric circles of 2^{m-n}-PSK, each circle having a radius of α^i, with $i = 0, 1, \ldots, 2^n - 1$. A typical value of the parameter α, referred to as *ring ratio*, is $\alpha = 2.0$ [1], and this value is adopted throughout the paper. Let a_k and ψ_k denote the amplitude and phase of X_k,

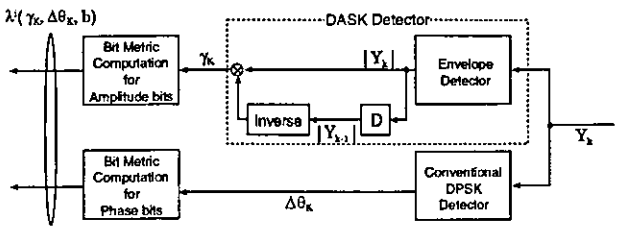

Fig. 2. Block diagram of the separative conventional differential detection.

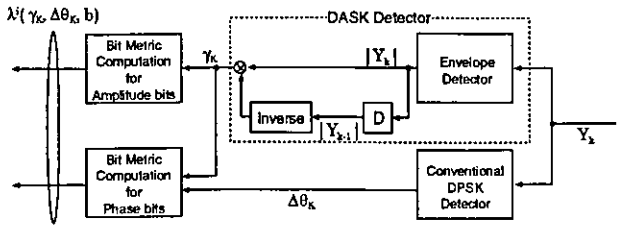

Fig. 3. Block diagram of the combinative conventional differential detection.

respectively. The first n bits of $\tilde{\mathbf{c}}_k$, $[\tilde{c}_k^1, \tilde{c}_k^2, \ldots, \tilde{c}_k^n]$, choose the amplitude difference between two successive symbols a_{k-1} and a_k. For 16-DAPSK system with $n = 1$, the coded bit $\tilde{c}_k^1 \in \{0, 1\}$ chooses $a_k \in \{1, \alpha\}$ by the following rule:

$$a_k = \begin{cases} a_{k-1} & \text{for } \tilde{c}_k^1 = 0 \\ \bar{a}_{k-1} & \text{for } \tilde{c}_k^1 = 1 \end{cases}$$

where $\bar{a}_k$ denotes flipping of a state of a_k i.e., $\bar{a}_k = 1$ or α for $a_k = \alpha$ or 1, respectively. For DPSK part, the remaining $(m - n)$ bits of $\tilde{\mathbf{c}}_k$, $[\tilde{c}_k^{n+1}, \tilde{c}_k^{n+2}, \ldots, \tilde{c}_k^m]$, choose the phase difference $\Delta\psi_k = \psi_k - \psi_{k-1}$ with Gray labeling [5].

B. Vector Channel Model

Throughout the paper, the channel is assumed to be frequency non-selective Rayleigh fading. The channel output Y_k corresponding to an input X_k can be expressed as

$$Y_k = \rho_k e^{j\phi_k} X_k + n_k, \tag{1}$$

where n_k is a complex additive white Gaussian noise (AWGN) with zero mean and variance $2\sigma^2$ per complex dimension, sampled at time instant k. The amplitude ρ_k and phase ϕ_k of a fading coefficient thus follows Rayleigh and uniform distributions, respectively.

In order to make theoretical analysis tractable, the following assumptions are introduced: First, the fading process is wide-sense stationary and slow enough to be time-invariant at least during two consecutive symbol intervals. Hence, it follows that $\rho_k = \rho_{k-1}$ and $\phi_k = \phi_{k-1}$ for any k. Second, the bit interleaving is ideal such that it fully eliminates fading correlations of consecutive bits after bitwise-deinterleaving at the receiver, i.e., the vector channel is *memoryless*.

C. Conventional Differential Detection

The simplest CDD for the DAPSK system consists of the two detectors which separately detect envelope and phase differences (see Fig. 2). To detect an envelope difference, the amplitude ratio γ_k is calculated by $\gamma_k = |Y_k/Y_{k-1}|$, where $|Y_k|$ denote an envelope sample of kth output symbol. Likewise, the phase difference is calculated by $\Delta\theta_k = \theta_k - \theta_{k-1}$, where $\theta_k = \angle Y_k$ and $\Delta\theta_k \in (-\pi, \pi)$. In this simplest scenario, γ_k and $\Delta\theta_k$ are separately used to determine the bit metric for amplitude and phase part, respectively. This approach, depicted in Fig. 2, will be called *separative CDD*,

With a little extra complexity, one may also incorporate the observed amplitude ratio γ_k to enhance the statistics of the phase bit metrics. The resultant receiver, which will be referred to as *combinative CDD*, is depicted in Fig. 3.

Let $\lambda^i(\gamma_k, \Delta\theta_k, b)$ denote the bit metric associated with the decision that ith bit of kth symbol is equal to b, where $i = 1, \cdots, m$ and $b \in \{0, 1\}$. In the case of separative CDD[1], the bit metrics of amplitude ($i \le n$) and phase ($n < i \le m$) may be calculated separately according to its respective output as follows:

$$\lambda^i(\gamma_k, \Delta\theta_k, b) = \begin{cases} \displaystyle\sum_{\{a_k, a_{k-1}\}_b^i} p(\gamma_k \mid a_k, a_{k-1}) & \text{for } i \le n, \\ \displaystyle\sum_{\{\Delta\psi_k\}_b^i} p(\Delta\theta_k \mid \Delta\psi_k) & \text{for } n < i \le m, \end{cases}$$

where the range of summation, $\{\boldsymbol{a}\}_b^i$, is over all the combinations of $\boldsymbol{a}$ of which the ith coded bit labeling is equal to b. A knowledge of probability density function (pdf) is necessary in the above equations, of which detailed derivations are placed in the Appendix. Bit metric calculation of combinative CDD can be implemented by suitably replacing with the corresponding pdf's in the above equation.

D. Multiple Symbol Differential Detection

In the case of MSDD, the ML metrics on multiple $(M-1)$ symbols $[X_k, X_{k-1}, \cdots, X_{k-(M-2)}]$ are calculated directly from observed M outputs $[Y_k, Y_{k-1}, \cdots, Y_{k-(M-1)}]$. Consequently, the complexity of a detector grows exponentially with M. To make a fair comparison in terms of delay constraint for each bit metric calculation, we choose the number of observed symbols $M = 2$ in the following. In this case, the total number of bit metrics needed to calculate for each m-coded-bit symbol is given by $m \cdot 2^{2m}$ since MSDD for DAPSK should be averaged over all possible reference symbols [4]. On the other hand, the corresponding total bit metrics required for the CDD-based systems is given by $n \cdot 2^n + (m-n) \cdot 2^{m-n}$. In the subsequent example, we choose $n = 1$ and $m = 4$. In this case, MSDD requires calculation of 1024 bit metrics, whereas that for CDD is 26.

III. Average Mutual Information

In this section, we numerically calculate the average mutual information (AMI) of the BICM-DAPSK systems on the assumption that the constellation alphabet X_k is chosen randomly from $\mathcal{X}$ with an equal probability. This quantity may be considered as a theoretical bound to the maximal information data rates achieved by the memoryless vector channel defined in section II-B. These values can be calculated

[1]Whenever necessary, we assume that a noise variance σ^2 is estimated perfectly at the receiver.

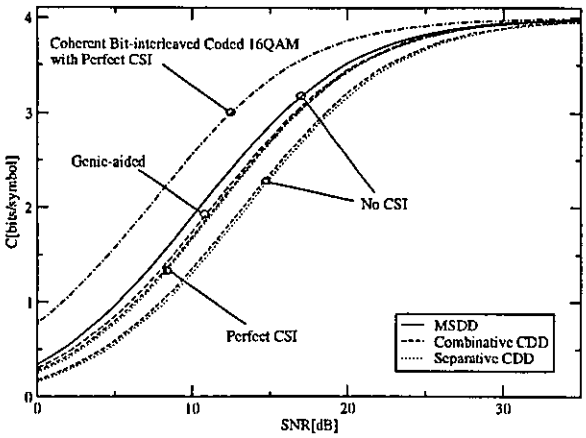

Fig. 4. Comparison of channel capacities of 16-level BICM over frequency non-selective Rayleigh fading channels.

based on the approach in [6], and details are omitted due to space limitation.

As shown in the following, the major loss of CDD in terms of the AMI, relative to MSDD, comes from the lack of amplitude reference in the phase bit metric calculation. Just for the purpose of comparison of this loss quantitatively, we introduce the following two ideal (and thus practically infeasible) receivers for the phase bit metric;

(a) **Perfect CSI receiver**: CSI ρ_k is known at the receiver, which will be used for phase bit metric calculation.
(b) **Genie-aided receiver**: CSI ρ_k *and* exact transmitted amplitudes $a_{k-1} = |X_{k-1}|$ and $a_k = |X_k|$ are known at the receiver, which will be used exclusively for phase bit metric calculation.

Fig. 4 shows the AMI of BICM with 16-DAPSK ($n = 1, m = 4$) constellation in conjunction with the separative or combinative CDD without CSI, perfect CSI, and genie-aided receivers. As a reference, the AMI of the DAPSK with MSDD ($M = 2$) without CSI [4], as well as that of the bit-interleaved 16-QAM with coherent reception and perfect CSI (and thus without any differential encoding) is shown [6].

By the data processing inequality [7], the AMI of the MSDD is always larger than that of the CDD, and the AMI of combinative CDD is always larger than that of separative CDD. Similarly, the AMI of the genie-aided receiver is always larger than that of the perfect CSI receiver. These relations are observed in Fig. 4.

From the figure, it is apparent that the loss of CDD due to the lack of CSI is considerable, whereas the AMI of the genie-aided receiver is close to that of MSDD. Thus, it can be conjectured that the superiority of MSDD comes from the fact that MSDD uses both amplitude and phase statistics to calculate each bit metric, whereas the CDD for DAPSK signaling deals with the amplitude and phase metrics independently. A removal of this statistical correlation results in the loss of the achievable AMI, which can be significantly recovered with the help of genie-aided receiver.

IV. New Bit Metrics for BICM-DAPSK over Raleigh Fading Channels

The comparative study on the AMI in the previous section suggests that the gap between the required SNR in order to achieve a certain information rate is noticeable. In other words, ignoring the knowledge of even partial CSI may significantly reduce the achievable information rate for a give SNR. Thus, if one can restore the CSI partially from the received symbol, it may lead to the performance improvement. Therefore, we wish to find a new bit metric that can approach the performance with *genie-aided* receiver by incorporating information from the detector. In fact, the output of the envelope detector can serve as an approximate CSI and transmitted amplitude, as proposed in [3]. While this approach has been applied to the empirical bit metric in conjunction with Gaussian approximation in [3], we develop improved bit metrics for Viterbi decoder and iterative MAP decoder, based on the *exact* pdf's derived in the Appendix.

A. Bit Metrics for Viterbi Decoder

1) Bit Metric for Amplitude: We start with a derivation of the bit metric for amplitude bits. Note that the direct application of (6) in the Appendix into bit metric calculation is quite complicated, since the calculation of the Bessel function is necessary. Furthermore, the knowledge of a noise variance σ^2 is required. Thus, we first use the following approximation

$$I_n(x) \approx \frac{1}{\sqrt{2\pi x}} \exp[x]$$

which becomes accurate for $x \gg n$. Then (6) in the Appendix can be rewritten as

$$\begin{aligned} p(\gamma_k \mid a_k, a_{k-1}, \rho_k) \approx (1+\gamma_k^2)^{-\frac{5}{2}} \left(2\pi\sigma^2\rho_k^2 a_k a_{k-1}\gamma_k\right)^{-\frac{1}{2}} \\ \times \left\{2\gamma_k\sigma^2(1+\gamma_k^2) + \gamma_k\rho_k^2(a_k\gamma_k + a_{k-1})^2\right\} \\ \times e^{\frac{-\rho_k^2}{2\sigma^2(1+\gamma_k^2)}(a_k - a_{k-1}\gamma_k)^2}. \end{aligned} \quad (2)$$

Multiplication of (2) by $2\sigma^2$ does not change the maximization in Viterbi decoding. Furthermore, the log-sum approximation $\log\sum_j z_j \approx \max_j \log z_j$ becomes accurate for high SNR [5], since in this case the summation in the left-hand side is dominated by the single maximum term. Thus, we substitute (2) with multiplication by $2\sigma^2$ into bit metric. Let $\tilde{\lambda}^i(\gamma_k, \Delta\theta_k, b \mid \rho_k)$, denote the corresponding log-domain bit metric. With log-sum approximation and dropping the constant terms, we obtain

$$\tilde{\lambda}^i(\gamma_k, \Delta\theta_k, b \mid \rho_k) \approx \max_{\{a_k, a_{k-1}\}_b^i} \left[-\frac{\rho_k^2}{(1+\gamma_k^2)}(a_k - a_{k-1}\gamma_k)^2\right].$$

Furthermore, inducing the approximation

$$\rho_k a_k \approx |Y_k|$$

which becomes also accurate for high SNR [3], we finally get

$$\tilde{\lambda}^i(\gamma_k, \Delta\theta_k, b \mid \rho_k) \approx \max_{\{\hat{r}_k\}_b^i} \left[\frac{-|Y_{k-1}|^2}{(1+\gamma_k^2)}(\gamma_k - \hat{r}_k)^2\right], \quad (3)$$

where $\hat{r}_k$ can be defined as $\hat{r}_k = a_k/a_{k-1}$. Note that the above bit metric exploits the envelope detector output $|Y_{k-1}|$, and the resultant block diagram is shown in Fig. 5.

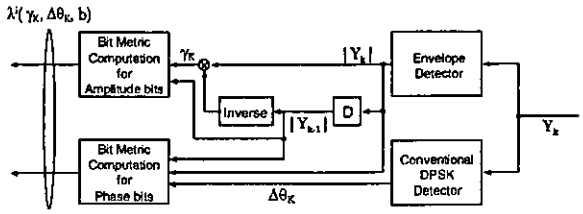

Fig. 5. Block diagram of the proposed receiver.

2) Bit Metric for Phase: From the AMI comparison in the previous section, γ_k and the output of envelope detector may be used in bit metric calculation to improve the performance. Using (5) in the Appendix with the same approximation procedure as the amplitude metric, we may write the bit metric as

$$\tilde{\lambda}^i(\gamma_k, \Delta\theta_k, b \mid \rho_k, a_k, a_{k-1}) \approx \max_{\Delta\psi^i_{b,k}} \left[\frac{|Y_k||Y_{k-1}|\gamma_k}{1+\gamma_k^2} \cos(\Delta\theta_k - \Delta\psi^i_{b,k}) \right]. \quad (4)$$

In the following simulation, we will make use of (3) and (4) for bit metric calculation.

B. Bit Metric for Iterative MAP Decoder

1) Bit Metric for Amplitude: With the pdf (2) and similar approximations above, the bit metric for amplitude bits can be obtained as

$$\lambda^i(\gamma_k, \Delta\theta_k, c_t \mid \rho_k) \approx \sum_{\hat{r}^i_{b,k}} (1+\gamma_k^2)^{-\frac{5}{2}} \left(2\pi\sigma^2|Y_{k-1}|^2\hat{r}\gamma_k\right)^{-\frac{1}{2}} \times \left(2\gamma_k\sigma^2(1+\gamma_k^2)+\gamma_k|Y_{k-1}|^2(\hat{r}_k\gamma_k+1)^2\right) e^{\frac{-|Y_{k-1}|^2}{2\sigma^2(1+\gamma_k^2)}(\gamma_k-\hat{r}_k)^2}.$$

2) Bit Metric for Phase: Likewise, based on (5) in the Appendix, the bit metric for phase bits can be obtained as

$$\lambda^i(\gamma_k, \Delta\theta_k, c_t \mid \rho_k, a_k, a_{k-1}) \approx \sum_{\Delta\psi^i_{k,b}} \frac{\gamma_k}{\pi(1+\gamma_k^2)^2} \times \left[1 + \frac{|Y_k|^2\gamma_k^2 + |Y_{k-1}|^2 + 2\gamma_k|Y_k||Y_{k-1}|\cos(\Delta\theta_k - \Delta\psi_k)}{2\sigma^2(1+\gamma_k^2)}\right] \times e^{-\frac{|Y_k|^2+|Y_{k-1}|^2\gamma_k^2-2|Y_k||Y_{k-1}|\gamma_k\cos(\Delta\theta_k-\Delta\psi_k)}{2\sigma^2(1+\gamma_k^2)}}$$

These bit metrics derived above are practically attractive, since they neither require the knowledge of CSI nor include any special function such as Bessel function.

V. Simulation Results

A. Differential Detection with Iterative MAP Decoder

The turbo codes are chosen as a channel encoder of BICM to show the performance of the proposed bit metrics for iterative MAP decoder. The coding rate of turbo codes is made 1/2 by puncturing [8], and interleaver size of turbo codes is 120000. The number of iteration for iterative MAP decoding is eighteen. Furthermore, ideal bit interleaver is assumed. Comparing the results in Fig. 6, it is observed that the performance loss of CDD with the proposed metric with respect to the genie-aided receiver is less than 0.2 dB, even within 0.5 dB of MSDD. Considering low complexity, the proposed metric with CDD may be an attractive alternative for the MSDD with $M = 2$.

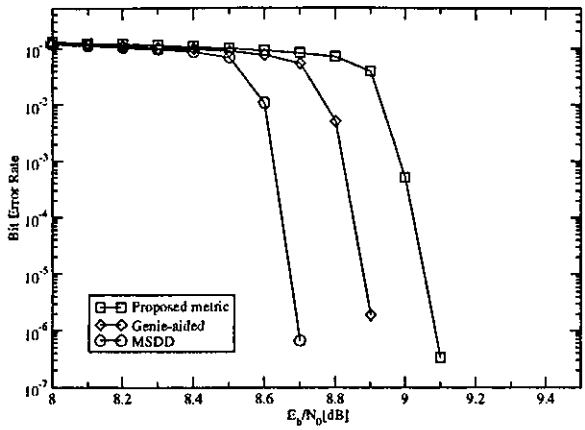

Fig. 6. Comparison of bit metrics for iterative MAP decoder.

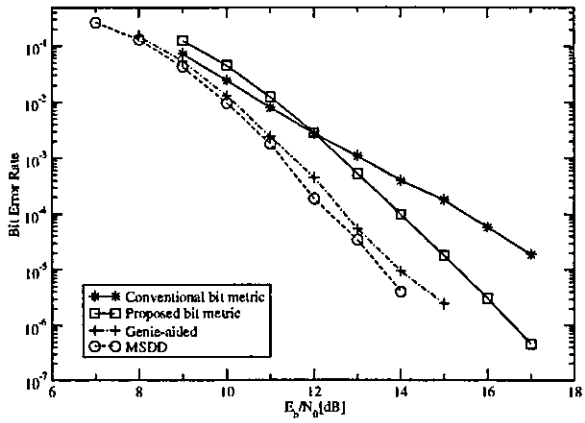

Fig. 7. Comparison of the bit metrics for Viterbi decoder.

B. Differential Detection with Viterbi Decoder

Simulations of the 16-DAPSK with the proposed metrics along with MSDD have been also performed with convolutional coding. The coding rate of the convolutional code is 1/2, its information size is 65536, and its generation matrix is (133, 171) in octal form. The ideal bit interleaver is assumed.

Fig. 7 shows the BER versus SNR per information bit (E_b/N_0) over frequency non-selective Rayleigh fading channels. The performance of the metric proposed in [3] is also shown as "conventional bit metric" in Fig. 7 for comparison. As observed, the gap between the proposed metric and genie-aided receiver is large, which may stem from the fact that the approximations used in deriving the proposed metric may not be accurate. However, it is observed that the proposed bit metric can significantly outperform that of [3] for a high SNR region, still retaining a simple receiver structure with low complexity metric calculation.

VI. Conclusions

In this paper, we have studied the bit-interleaved coded DAPSK over frequency non-selective Rayleigh fading chan-

nels. We first derived the exact bit metrics of separative and combinative CDD and compared them with MSDD in terms of the AMI, thereby revealing the theoretical loss due to the use of CDD quantitatively. Furthermore, based on the AMI results, a new bit metric for CDD-based system has been proposed. Simulation results have shown that the proposed metric can improve performance significantly without significantly increasing computational cost.

APPENDIX

In this Appendix, we derive the exact pdf's of the amplitude ratio γ_k and phase difference $\Delta\theta_k$ for given channel statistics. They are required to calculate the metrics as well as the AMI in the paper.

A. Probability Density Function without CSI

We start with the derivation of the pdf in the absence of CSI ρ_k.

1) Amplitude Ratio: Conditioned that two consecutive symbols X_{k-1} and X_k are transmitted, the conditional joint pdf of two received consecutive symbols is given by

$$p(Y_k, Y_{k-1} \mid X_k, X_{k-1}, \rho_k, \rho_{k-1}, \phi_k, \phi_{k-1}) = \frac{1}{(2\pi\sigma^2)^2} e^{-\frac{1}{2\sigma^2}\{|Y_k-\rho_k X_k e^{j\phi_k}|^2+|Y_{k-1}-\rho_{k-1}X_{k-1}e^{j\phi_{k-1}}|^2\}}$$

Considering the vector channel model assumed in Section II-B and changing the variables appropriately, we obtain (see, e.g., [9])

$$p(\gamma_k, \Delta\theta_k \mid a_k, a_{k-1}, \Delta\psi_k, \rho_k) = \frac{\gamma_k}{\pi(1+\gamma_k^2)^2}\left[1+\frac{\rho_k^2}{2\sigma^2(1+\gamma_k^2)}\left\{a_k^2\gamma_k^2+a_{k-1}^2+2\gamma_k a_k a_{k-1}\cos(\Delta\theta_k-\Delta\psi_k)\right\}\right] \times e^{-\frac{\rho_k^2}{2\sigma^2(1+\gamma_k^2)}\left\{a_k^2+a_{k-1}^2\gamma_k^2-2a_k a_{k-1}\gamma_k\cos(\Delta\theta_k-\Delta\psi_k)\right\}}. \quad (5)$$

where $a_k = |X_k|$. By integrating out ρ_k and $\Delta\theta_k$ in (5), we obtain

$$p(\gamma_k \mid a_k, a_{k-1}) = \frac{4\sigma^2\gamma_k\left(a_k^2+a_{k-1}^2+2\sigma^2\right)\left(a_k^2+2\sigma^2+(a_{k-1}^2+2\sigma^2)\gamma_k^2\right)}{z_k\left(a_k^2+2\sigma^2+2a_k a_{k-1}\gamma_k+(a_{k-1}^2+2\sigma^2)\gamma_k^2\right)^3}$$

where

$$z_k \triangleq \left(1-\frac{4a_k a_{k-1}\gamma_k}{a_k^2+2\sigma^2+2a_k a_{k-1}\gamma_k+(a_{k-1}^2+2\sigma^2)\gamma_k^2}\right)^{3/2}.$$

2) Phase Difference: The pdf of the phase difference between two DAPSK modulated symbols can be obtained by integrating out γ_k in (5), yielding

$$p(\Delta\theta_k \mid a_k, a_{k-1}, \Delta\psi_k) = \frac{\sigma^2(a_k^2+a_{k-1}^2+2\sigma^2)}{\pi\xi_k(a_{k-1}^2+2\sigma^2)} \times \left\{2(a_{k-1}^2+2\sigma^2)+a_k a_{k-1}\cos(\Delta\theta_k-\Delta\psi_k)\cdot\Lambda_k\right\},$$

where

$$\Lambda_k \triangleq \frac{1}{\eta_k}2(a_{k-1}^2+2\sigma^2)\arctan\left[\frac{a_k a_{k-1}\cos(\Delta\theta_k-\Delta\psi_k)}{\eta_k}\right]+\pi(a_{k-1}^2+2\sigma^2),$$

$$\eta_k \triangleq \sqrt{(a_k^2+2\sigma^2)(a_{k-1}^2+2\sigma^2)-a_k^2a_{k-1}^2\cos(\Delta\theta_k-\Delta\psi_k)^2},$$

$$\xi_k \triangleq 4\sigma^2(a_{k-1}^2+2\sigma^2)+a_k^2(a_{k-1}^2+4\sigma^2)-a_k^2a_{k-1}^2\cos[2(\Delta\theta_k-\Delta\psi_k)].$$

B. Probability Density Function with CSI

1) Amplitude Ratio: As a reference, if CSI ρ_k is known at the receiver, the corresponding pdf can be obtained by integrating $\Delta\theta_k$ in (5) from $-\pi$ to π. The result can be expressed as

$$p(\gamma_k \mid a_k, a_{k-1}, \rho_k) = \frac{2\gamma_k}{(1+\gamma_k^2)^2}e^{-\frac{\rho_k^2}{2\sigma^2(1+\gamma_k^2)}\left\{a_k^2+a_{k-1}^2\gamma_k^2\right\}}I_0\left(\frac{\rho_k^2 a_k a_{k-1}\gamma_k}{\sigma^2(1+\gamma_k^2)}\right) + \frac{\gamma_k\rho_k^2(a_k^2\gamma_k^2+a_{k-1}^2)}{\sigma^2(1+\gamma_k^2)^3}e^{-\frac{\rho_k^2}{2\sigma^2(1+\gamma_k^2)}\left\{a_k^2+a_{k-1}^2\gamma_k^2\right\}}I_0\left(\frac{\rho_k^2 a_k a_{k-1}\gamma_k}{\sigma^2(1+\gamma_k^2)}\right) + \frac{2\gamma_k^2\rho_k^2 a_k a_{k-1}}{\sigma^2(1+\gamma_k^2)^3}e^{-\frac{\rho_k^2}{2\sigma^2(1+\gamma_k^2)}\left\{a_k^2+a_{k-1}^2\gamma_k^2\right\}}I_1\left(\frac{\rho_k^2 a_k a_{k-1}\gamma_k}{\sigma^2(1+\gamma_k^2)}\right) \quad (6)$$

where $I_n(\cdot)$ is the modified Bessel function of the first kind with the nth order.

2) Phase Difference: In this case, a closed from pdf cannot be obtained directly from (5). An alternative solution based on the characteristic function (see, e.g., [10]) results in

$$p(\Delta\theta_k \mid a_k, a_{k-1}, \Delta\psi_k, \rho_k) = \frac{1}{4\pi} \times \int_0^\pi \sin\alpha\left[1+U_k+V_k\cos\alpha+W_k\sin\alpha\cos(\Delta\theta_k-\Delta\psi_k)\right] \times \exp[V_k\cos\alpha+W_k\sin\alpha\cos(\Delta\theta_k-\Delta\psi_k)-U_k]d\alpha,$$

where $U_k = \frac{\rho_k^2}{4\sigma^2}(a_k^2+a_{k-1}^2)$, $V_k = \frac{\rho_k^2}{4\sigma^2}(a_k^2-a_{k-1}^2)$, $W_k = U_k^2-V_k^2$. Further simplification of the above integration appears difficult to carry out and thus one may resort to numerical integration.

REFERENCES

[1] H. Rohling and V. Engels, "Differential amplitude phase shift keying (DAPSK) - a new modulation method for DTVB," in *Proc. Int. Broadcasting Convention*, (Amsterdam, The Netherlands), pp. 102–108, 1995.

[2] D. Divsalar and M. K. Simon, "Multiple-symbol differential detection of MPSK," *IEEE Trans. Commun.*, vol. 38, pp. 300–308, Mar. 1990.

[3] T. May, H. Rohling, and V. Engels, "Performance analysis of Viterbi decoding for 64-DAPSK and 64-QAM modulated OFDM signals," *IEEE Trans. Commun.*, vol. 46, pp. 182–190, Feb. 1998.

[4] R. F. Fischer, L. H.-J. Lampe, and S. H. Muller-Weinfurtner, "Coded modulation for noncoherent reception with application to OFDM," *IEEE Trans. Veh Technol.*, vol. 50, pp. 901–919, July 2001.

[5] E. Zehavi, "8-PSK trellis codes for a Rayleigh channel," *IEEE Trans. Commun.*, vol. 40, pp. 873–884, May 1992.

[6] G. Caire, G. Taricco, and E. Biglieri, "Bit-interleaved coded modulation," *IEEE Trans. Inform. Theory*, vol. 44, pp. 927–946, May 1998.

[7] T. M. Cover and J. A. Thomas, *Elements of Information Theory*. New york: John Wiley & Sons, Inc., 1991.

[8] C. Berrou, A. Glavieux, and P. Thitimajshima, "Near Shannon limit error-correcting coding and decoding: turbo-codes," in *Proc. of IEEE ICC'93*, (Geneva, Switzerland), pp. 1064–1070, May 1993.

[9] T. Suzuki and T. Mizuno, "Multiple-symbol differential detection scheme for differential amplitude modulation," in *Proc. of IZS'94 (International Zurich Seminar on Digital Communications)*, (Zurich, Switzerland), pp. 326–337, 1994.

[10] R. F. Pawula, S. O. Rice, and J. H. Roberts, "Distribution of the phase angle between two vectors perturbed by Gaussian noise," *IEEE Trans. Commun.*, vol. COM-30, pp. 1828–1841, Aug. 1982.

Band-Limited Frequency Efficient Orthogonal Pulse Shape Modulation for UWB Communications

Alex Cartagena Gordillo, Giuseppe Thadeu Freitas de Abreu and Ryuji Kohno
Division of Electrical and Computer Engineering, Yokohama National University
E-mails: [alex, giuseppe, kohno]@kohnolab.dnj.ynu.ac.jp

Abstract—**This paper presents a study about the design of an equally frequency limited set of orthogonal pulses, adequate for an Impulse Radio (IR) Ultra Wideband (UWB) communication system employing Pulse Shape Modulation (PSM). UWB systems have to face many spectrum restrictions like avoiding interference to existing systems or comply with spectrum mask regulations like the one emitted by the Federal Communications Commission (FCC). Then, UWB systems have to restrict their bandwidth and maximize its usage efficiency. The proposed set of pulses meets such requirements and provides additional robustness when interference to narrowband systems should be avoided.**

I. Introduction

Ultra wideband (UWB) communication systems have to face many spectrum restriction to avoid interference or comply with regulations. Then, UWB systems have to restrict their bandwidth and maximize its usage efficiency. However, limited bandwidth degrades the maximum transmission rate of the system. Using many pulses synchronized to form an orthogonal system, and modulated using Pulse Shape Modulation (PSM) was proposed in [1]. Pulses designed in this way can increase the capacity of the system.

As mentioned in [2], the transmit and receive antennae produce derivative effects on the transmit and receive UWB pulse shapes. Then, the pulse shape at the output of the receive antenna should be the second derivative of the transmit pulse shape. In this study, in order to concentrate our analysis in the band limited set of pulses, these derivative effects will not be considered. On the other hand, as it is discussed in [3], the results obtained in this study can be combined with the results in [4], as a result both frequency limitation and derivative effects can be overcame without losing the validity of the present analysis.

In order to focus our attention on the characteristics of the proposed pulse shapes, we assume in that all the operations occur after synchronization between transmitter and receiver has been achieved.

The contents of the remainder of this paper are organized as follows: in section 2, we review basic concepts of Hermite pulses and Pulse Shape Modulation. The proposed set of pulses are derived in section 3, section 4 illustrates some simulation results and finally some conclusions complete our paper.

II. Hermite Pulses and Pulse Shape Modulation

A. Hermite pulses

Hermite functions and Hermite polynomials have been studied extendedly in the past, as it is mentioned in [1]. Hermite functions for UWB PSM communications, as defined in [5], are mathematically described as

$$\psi_n(t) = \frac{H_n(t)e^{-\frac{t^2}{2}}}{\sqrt{2^n n!\sqrt{\pi}}}, \tag{1}$$

where $H_n(t)$ are the Hermite polynomials. The Fourier Transform of these pulses is represented by

$$\Psi_{n+1}(\omega) = \sqrt{\frac{2}{n+1}} j\omega \Psi_n(\omega) + \sqrt{\frac{n}{n+1}} \Psi_{n-1}(\omega). \tag{2}$$

B. Pulse Shape Modulation

Pulse Shape Modulation is an alternative impulse radio system, different from the IR described in [2], it is based in the orthogonality of pulse shapes as proposed in [1] and [5]. Basically, information bits 1 and 0 are represented by two different orthogonal pulses. This idea can be extended to a M-ary modulation scheme using M orthogonal pulse waveforms.

III. Design of Frequency Limited Pulses

A. Scaling Factors Determination

The upper frequency limit of the Hermite pulses increases with the increase in the order of the Hermite polynomials. To use the spectrum efficiently, a set of orthogonal pulses with the same upper frequency limit is desired. To determine the upper frequency limit of our system, we refer to the bandwidth definition. There are many definitions of bandwidth, but we are going to assume the one adopted by the FCC [6], which is called Fractional Power Containment Bandwidth. It states that the occupied bandwidth is the band that leaves exactly 0.5% of the signal power above the upper band limit and exactly 0.5% of the signal power below the lower band limit. Thus 99% of the signal power is inside the occupied band [6]. With this purpose, the Energy Spectral Density of a Hermite pulse shape is calculated as

$$E_n = \frac{1}{2\pi} \int_{-\infty}^{\infty} |\Psi(\omega)|^2 d\omega. \tag{3}$$

In addition from Parseval's theorem for continuous signals we have

$$\int_{-\infty}^{\infty} |\psi(t)|^2 dt = \frac{1}{2\pi} \int_{-\infty}^{\infty} |\Psi(\omega)|^2 d\omega, \tag{4}$$

0-7803-8408-3/04/$20.00 © 2004 IEEE

this implies that limiting the upper frequency of a Hermite pulse shape requires a modification of its pulse width. However, for different orders of Hermite pulses, different modifications of the pulse widths are necessary. Even though the modifications introduced in the pulses widths generates equally spectrum-limited pulses, the new set of pulses lose mutual orthogonality and PSM can not be used anymore. To overcome this problem we invoke the orthogonalization procedures employed in [4] and [7]. Pulse width modifications can be obtained including a pulse width scaling factor α in (1), such that it becomes

$$\varphi_n(t,\alpha) = \Upsilon_n \frac{H_n(\alpha t)e^{-\frac{(\alpha t)^2}{2}}}{\sqrt{2^n n!\sqrt{\pi}}}. \quad (5)$$

Additionally, Υ_n is introduced as an amplitude limiting factor which helps to normalize the pulse energy to unity. Through the analysis, it was found that $\Upsilon_n = \sqrt{\alpha}$ for any value of n. To simplify our analysis without losing generality, we assume α to be a real positive number. The Fourier transform of successive orders of width-modified Hermite pulses, described by (5), are related by the following recurrent relationship

$$\Phi_{n+1}(\alpha,\omega) = \sqrt{\tfrac{n}{n+1}}\Phi_{n-1}(\alpha,\omega) - \tfrac{j\omega}{\alpha}\sqrt{\tfrac{2}{n+1}}\Phi_n(\alpha,\omega). \quad (6)$$

The Fourier transform of the first two width-modified Hermite pulse shapes are described by

$$\Phi_0(\alpha,\omega) = \sqrt{\frac{2\sqrt{\pi}}{\alpha}}e^{\left(-\frac{\omega^2}{2\alpha^2}\right)}, \quad (7)$$

$$\Phi_1(\alpha,\omega) = -2j\omega\sqrt{\frac{\sqrt{\pi}}{\alpha^3}}e^{\left(\frac{\omega^2}{2\alpha^2}\right)}. \quad (8)$$

Using (3), we can find the energy of the *nth* order width-modified Hermite pulses, limited to the frequency γ, as follows

$$E_n(\alpha) = \frac{1}{\pi}\int_0^{\gamma} |\Phi(\alpha,\omega)|^2 d\omega. \quad (9)$$

Making

$$E_n(\alpha) = \frac{0.99}{\pi}\int_0^{\infty} |\Phi(\alpha,\omega)|^2 d\omega, \quad (10)$$

we have found implicit functions of γ and α, which are graphically presented in Fig. 1, and are approximated by (11) for $\alpha_n > 0$.

$$\begin{aligned} \gamma_0(\alpha_0) &= 0.2899\alpha_0 \\ \gamma_1(\alpha_1) &= 0.3791\alpha_1 \\ \gamma_2(\alpha_2) &= 0.4471\alpha_2 \\ \gamma_3(\alpha_3) &= 0.5047\alpha_3 \end{aligned} \quad (11)$$

From (11), for any arbitrary upper frequency limit γ_c, a set of scaling factors α_n can be found that modify the n Hermite pulses which upper frequency limit is γ_c. Fig. 2 shows an example of width-modified Hermite pulses spectrum of such pulses. Clearly, all the frequency limits of the pulses spectrum in Fig. 2 are the same, in contrast with the spectrum of the

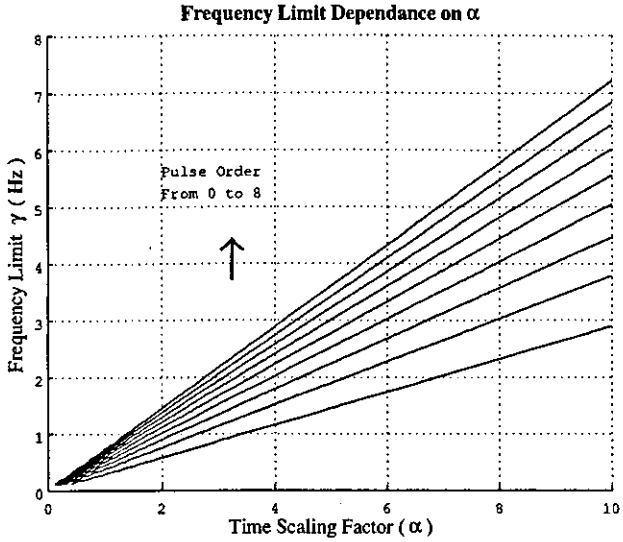

Fig. 1. Frequency as a function of the time scaling factor α_n for Hermite pulses of orders from 0 to 8

original Hermite functions, which have different frequency limits. However, as mentioned before, these modified pulse shapes are not orthogonal anymore, this problem will be addressed in the next section.

B. Orthogonalization Procedure

For orthogonalization purposes we are going to adopt the same procedure used in [4], then two versions of orthogonal set of pulses can be generated from the conventional Hermites, one used in a Matched type receiver and the other in a Non-Matched type receiver. This classification depends on whether the receive template is matched or not to the transmit pulse shape. For the Non-Matched case, the receive template consists on the original Hermite pulses. Let's assume an ideal noiseless UWB communication channel. The number of pulses are given by an alphabet of N pulses. Additionally, let the only distorting element between the transmitter and the bank of correlators at the receiver be a pseudo-channel given by a matrix $\mathbf{C}$, defined as

$$\mathbf{C} = \begin{pmatrix} c_{0,0} & c_{0,1} & \cdots & c_{0,N-1} \\ c_{1,0} & c_{1,1} & \cdots & c_{1,N-1} \\ \vdots & \vdots & \ddots & \vdots \\ c_{N-1,0} & c_{N-1,1} & \cdots & c_{N-1,N-1} \end{pmatrix}. \quad (12)$$

The value of $c_{n,m}$ depends on the type of receiver used, for the Matched receiver it is given by the correlation between the upper-frequency limited Hermite pulses given by (5), and is defined as

$$c^M_{n,m} = \int_{-\infty}^{\infty} \varphi_n(t,\alpha_n)\varphi_m(t,\alpha_m)dt, \quad (13)$$

where M stands for Matched, $m,n \in \{0,...,N-1\}$, and $c^M_{n,m} = 1$ for $m = n$, and different values for $m \neq n$.